

Supporting Information

Bioinspired Models for an Unusual 3-Histidine Motif of Diketone Dioxygenase Enzymes

*Ramamoorthy Ramasubramanian,^a Karunanithi Anandababu,^a Nadia C. Mösch-Zanetti,^b
Ferdinand Belaj^b and Ramasamy Mayilmurugan^{a*}*

^aBioinorganic Chemistry Laboratory/Physical Chemistry, School of Chemistry, Madurai Kamaraj University, Madurai 62502, India. ^bInstitute of Chemistry, University of Graz, Schubertstrasse 1, 8010 Graz, Austria.

Crystal Structure: In this unit cell the anion including S3 would lie on an inversion centre but no disorder of this anion is detectable. Furthermore, in this centrosymmetric unit cell the anion including S4 and the acetonitrile solvent molecule (including N8) would lie on opposite sides of an inversion centre. Therefore, if the structure as a whole were centrosymmetric, strong difference peaks from the S atoms in the vicinity of C30 as well as in the space occupied by this acetonitrile solvent molecule would remain. Since this is not the case, the crystal structure is non-centrosymmetric. The CF₃ group of the anion in the largest void (including S4) was disordered over two orientations (Fig. S1).

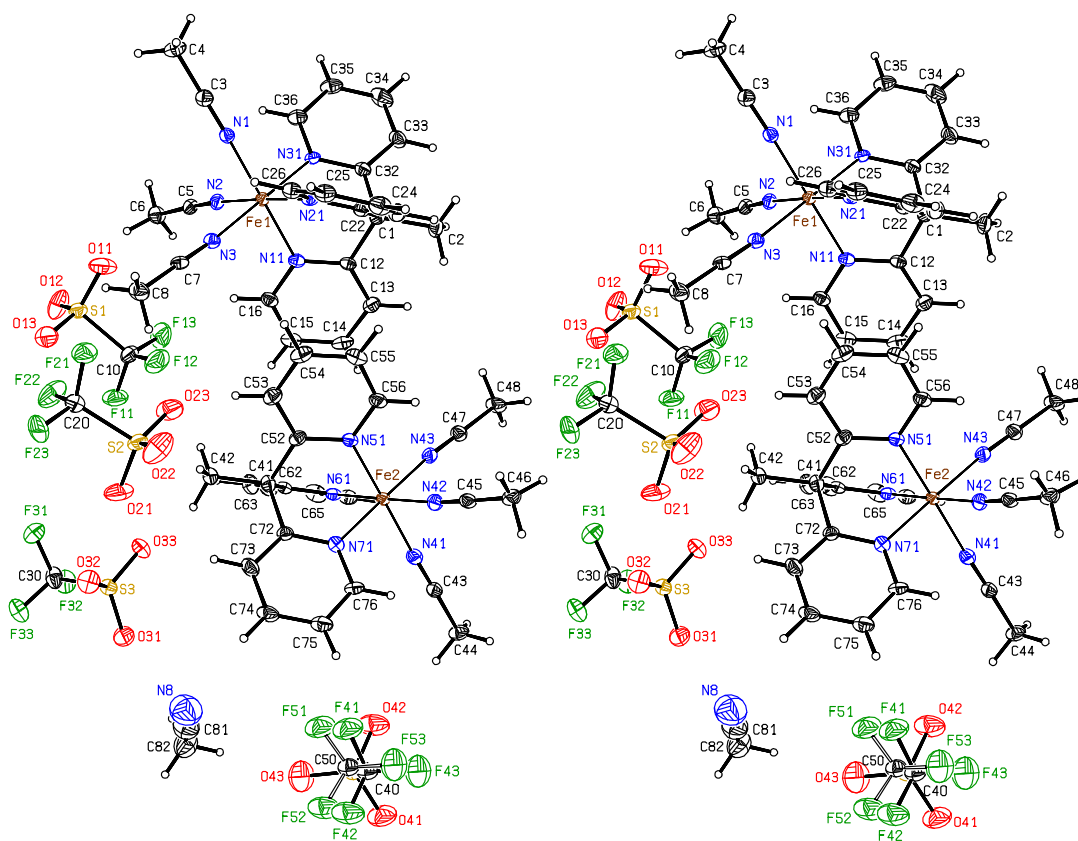


Figure S1. Stereoscopic ORTEP plot of the asymmetric unit of **1** showing the atomic numbering scheme. The probability ellipsoids are drawn at the 50% probability level. The H atoms are drawn with arbitrary radii, the bonds to atoms with site occupation factors less than 0.5 are plotted with open bonds.

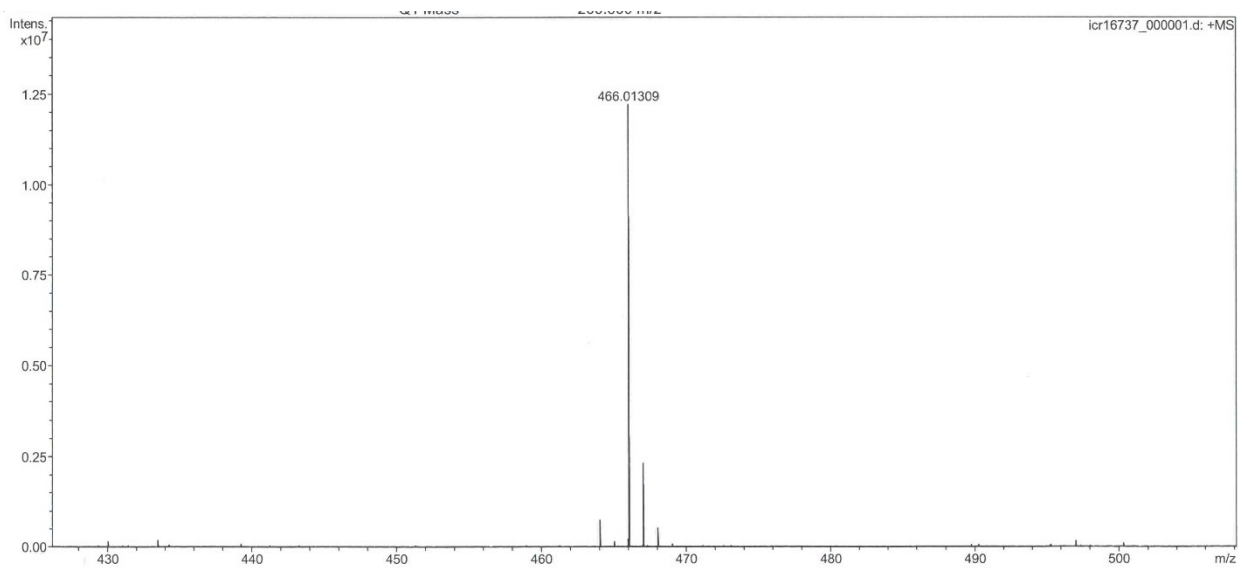


Figure S2. The HR-ESI mass spectra for $[\text{Fe}(\text{L1})(\text{SO}_3\text{CF}_3)]\text{SO}_3\text{CF}_3$, **1** in acetonitrile.

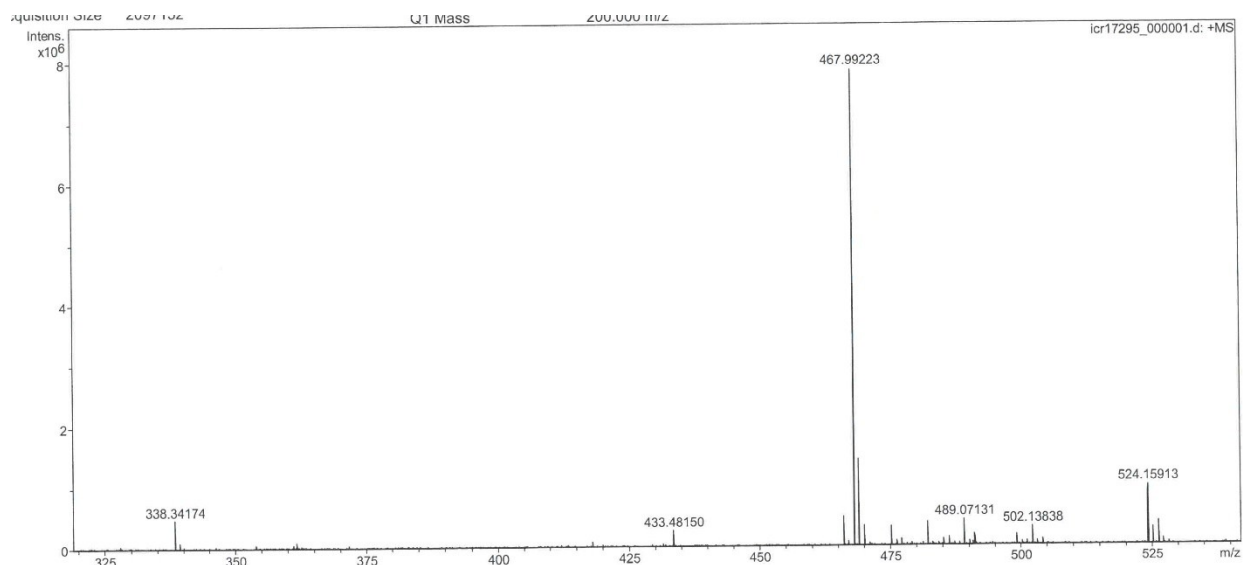


Figure S3. The HR-ESI mass spectra for $[\text{Fe}(\text{L2})(\text{SO}_3\text{CF}_3)]\text{SO}_3\text{CF}_3$, **2** in acetonitrile.

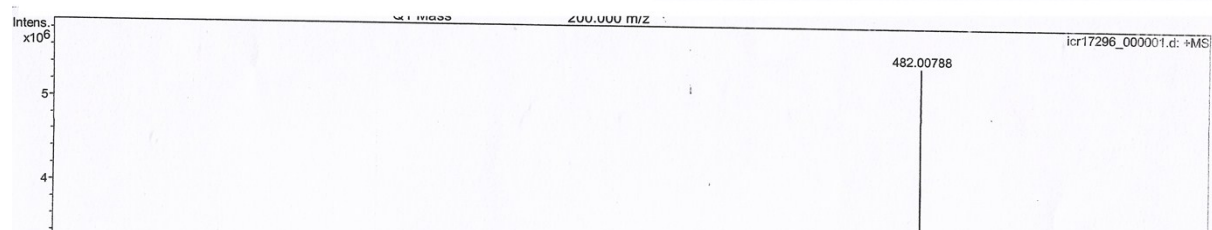


Figure S4. The HR-ESI mass spectra for $[\text{Fe}(\text{L}3)(\text{SO}_3\text{CF}_3)]\text{SO}_3\text{CF}_3$, **3** in acetonitrile.

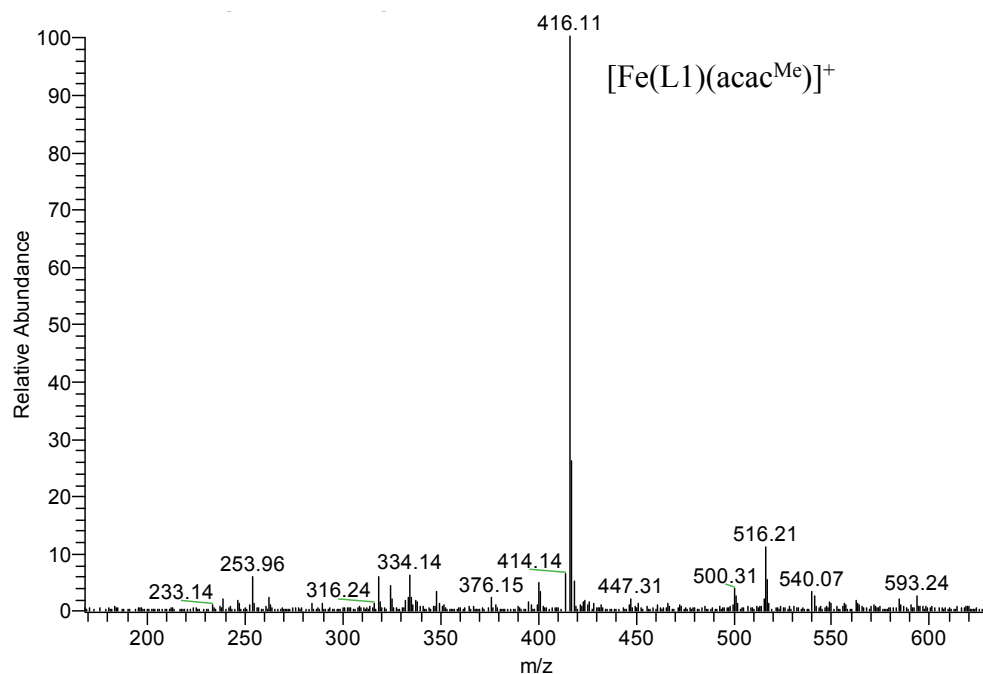
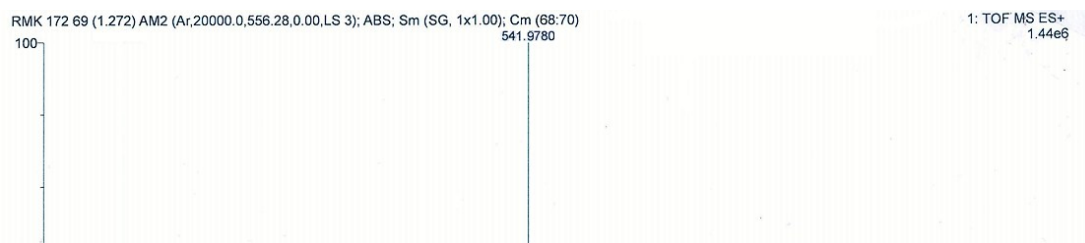


Figure S5. The ESI-MS spectra of $[\text{Fe}(\text{L}1)(\text{acac}^{\text{Me}})]^+$ for **1a** in acetonitrile.



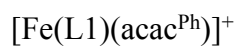


Figure S6. The ESI-MS spectra of $[\text{Fe}^{\text{II}}(\text{L1})(\text{acac}^{\text{Ph}})]^+$ for **1b** in acetonitrile.

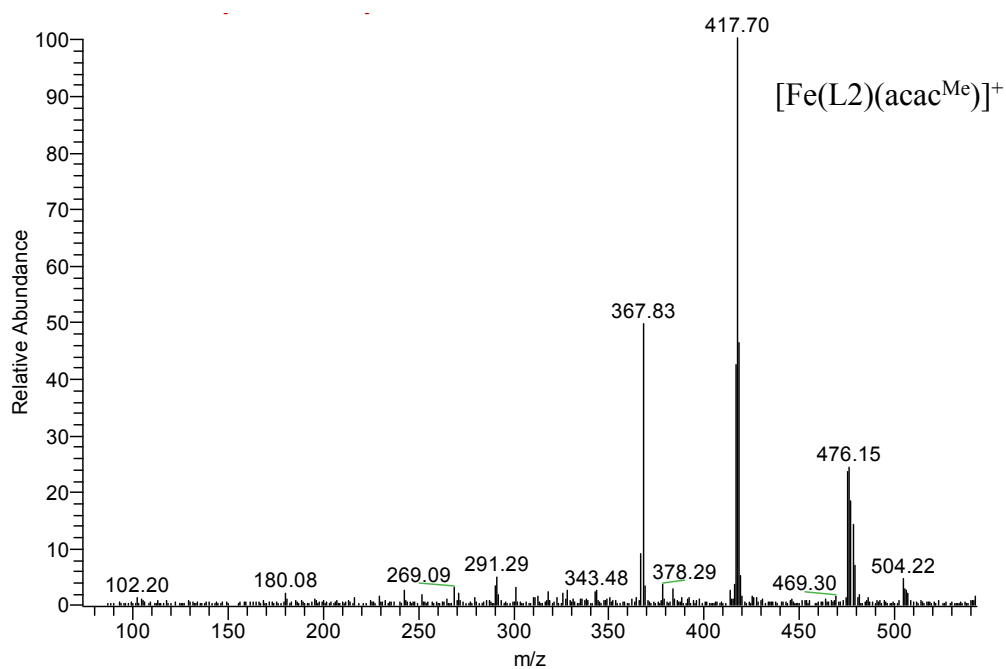


Figure S7. The ESI-MS spectra of $[\text{Fe}(\text{L2})(\text{acac}^{\text{Me}})]^+$ for **2a** in acetonitrile.

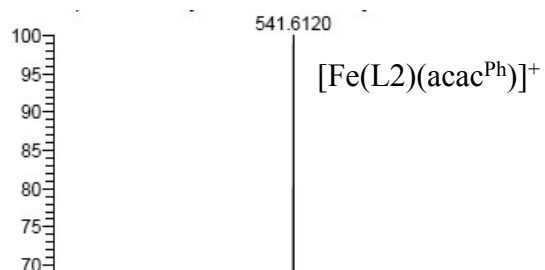


Figure S8. The The HR-ESI mass spectra spectra of $[\text{Fe}^{\text{II}}(\text{L2})(\text{acac}^{\text{Ph}})]^+$ for **2b** in acetonitrile.

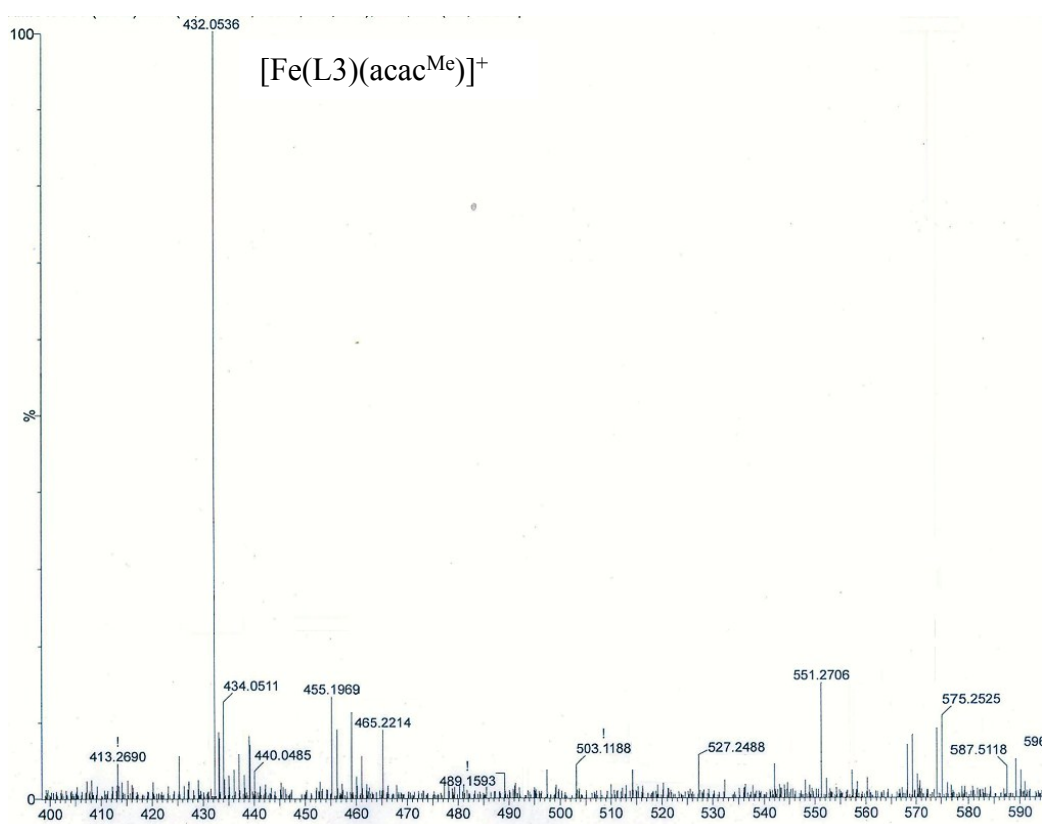


Figure S9. The The HR-ESI mass spectra of $[\text{Fe}(\text{L3})(\text{acac}^{\text{Me}})]\text{SO}_3\text{CF}_3$ for **3a** in acetonitrile.

1a

2a

Figure S10. FT-IR spectra of **1a – 3a**

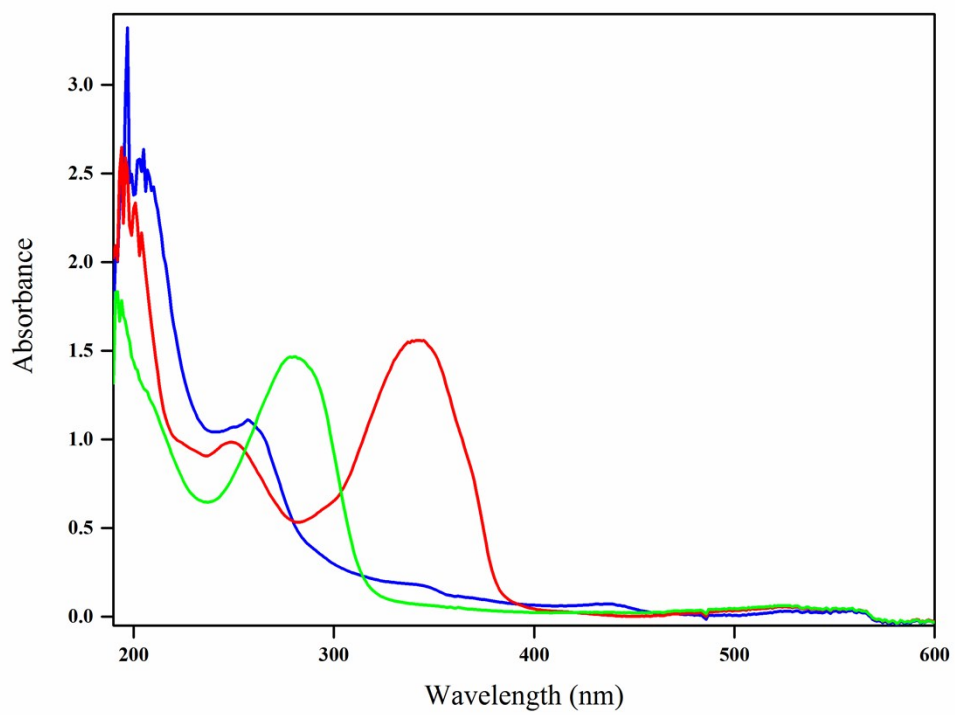


Figure S11. The electronic spectra of $[\text{Fe}(\text{L1})(\text{SO}_3\text{CF}_3)]\text{SO}_3\text{CF}_3$ **1** (blue), $\text{Fe}(\text{L1})(\text{acac}^{\text{Me}})]\text{SO}_3\text{CF}_3$, **1a** (green) and $[\text{Fe}(\text{L1})(\text{acac}^{\text{Ph}})]\text{SO}_3\text{CF}_3$, **1b** (red) (1×10^{-7} M) in acetonitrile.

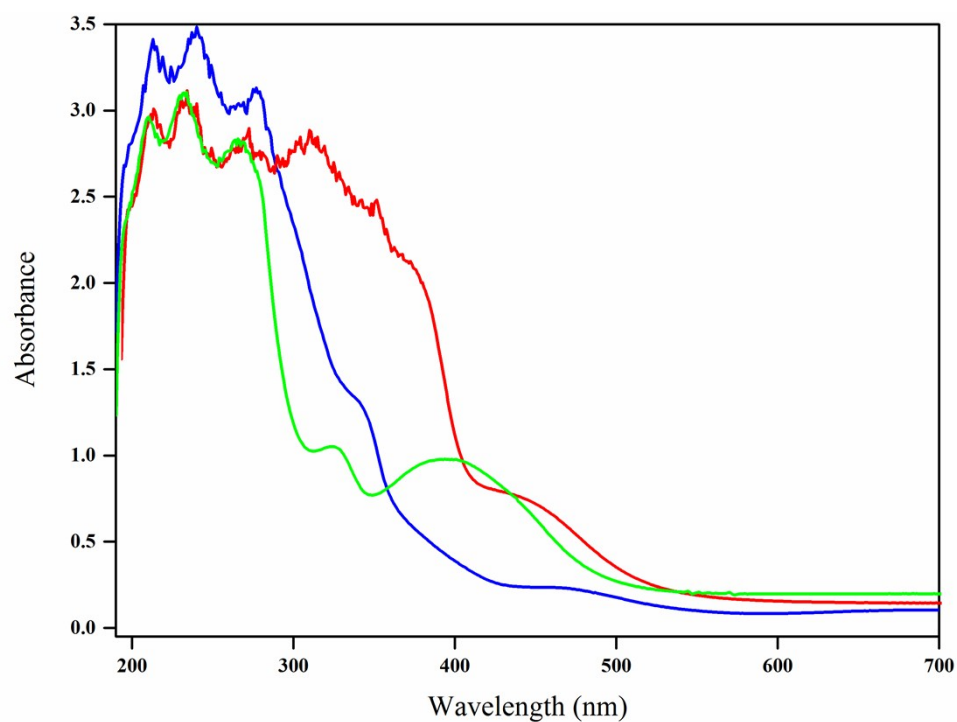


Figure S12. The electronic spectra of $[\text{Fe}(\text{L2})(\text{SO}_3\text{CF}_3)]\text{SO}_3\text{CF}_3$ **2** (blue), $[\text{Fe}(\text{L2})(\text{acac}^{\text{Me}})]\text{SO}_3\text{CF}_3$, **2a** (green) and $[\text{Fe}(\text{L2})(\text{acac}^{\text{Ph}})]\text{SO}_3\text{CF}_3$, **2b** (red) (1×10^{-3} M) in acetonitrile.

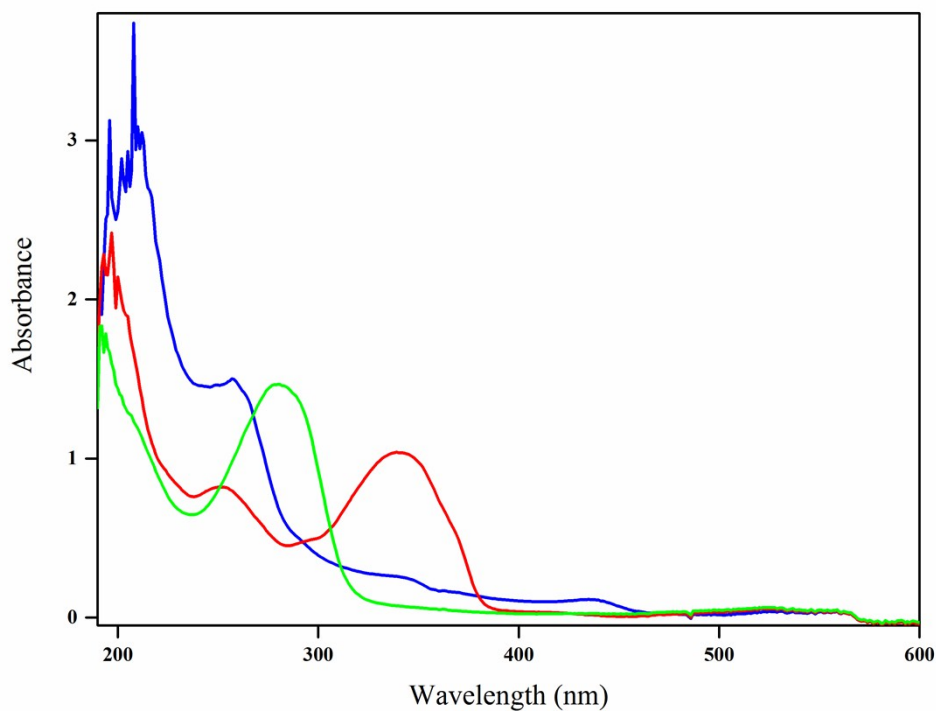


Figure S13. Electronic spectra of $[\text{Fe}(\text{L}2)(\text{SO}_3\text{CF}_3)]\text{SO}_3\text{CF}_3$ **2** (blue), $[\text{Fe}(\text{L}2)(\text{acac}^{\text{Me}})]\text{SO}_3\text{CF}_3$, **2a** (green) and $[\text{Fe}(\text{L}2)(\text{acac}^{\text{Ph}})]\text{SO}_3\text{CF}_3$, **2b** (red) (1×10^{-7} M) in acetonitrile.

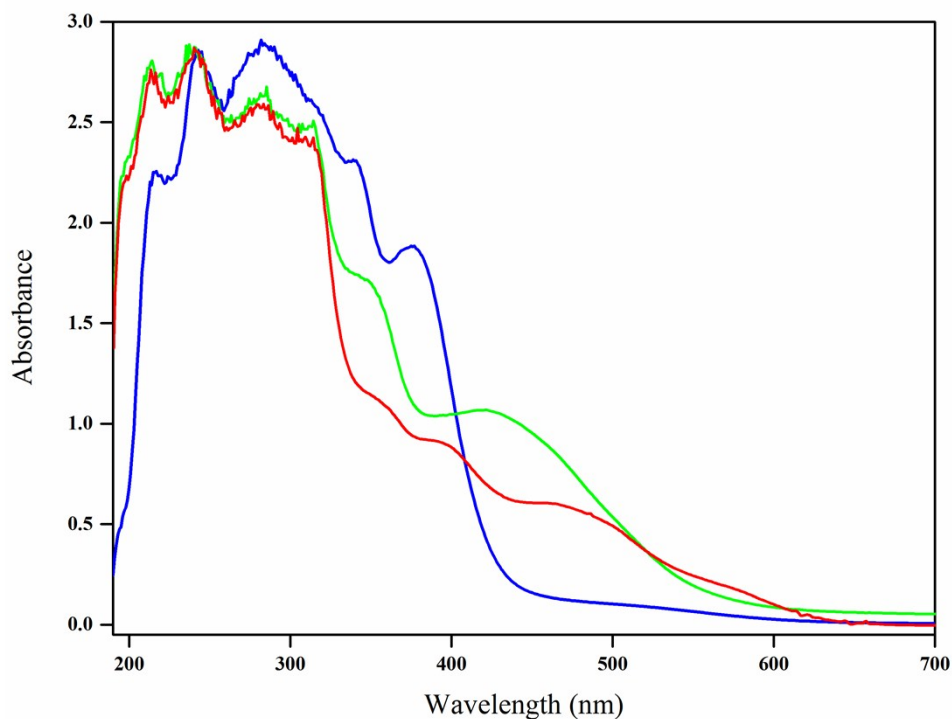


Figure S14. The electronic spectra of $[\text{Fe}(\text{L}3)(\text{SO}_3\text{CF}_3)]\text{SO}_3\text{CF}_3$ **3** (blue), $[\text{Fe}(\text{L}3)(\text{acac}^{\text{Me}})]\text{SO}_3\text{CF}_3$, **3a** (green) and $[\text{Fe}(\text{L}3)(\text{acac}^{\text{Ph}})]\text{SO}_3\text{CF}_3$, **3b** (red) (1×10^{-3} M) in acetonitrile.

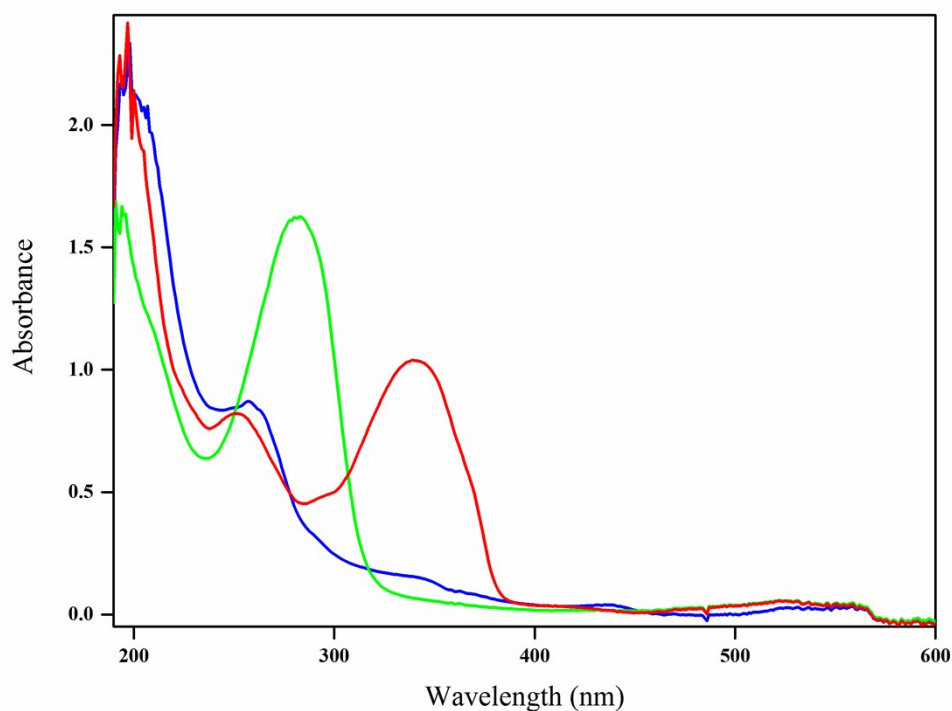


Figure S15. The electronic spectra of $[\text{Fe}(\text{L3})(\text{SO}_3\text{CF}_3)]\text{SO}_3\text{CF}_3$ **3** (blue), $[\text{Fe}(\text{L3})(\text{acac}^{\text{Me}})]\text{SO}_3\text{CF}_3$, **3a** (green); $[\text{Fe}(\text{L3})(\text{acac}^{\text{Ph}})]\text{SO}_3\text{CF}_3$, **3b** (red) (1×10^{-7} M) in acetonitrile.

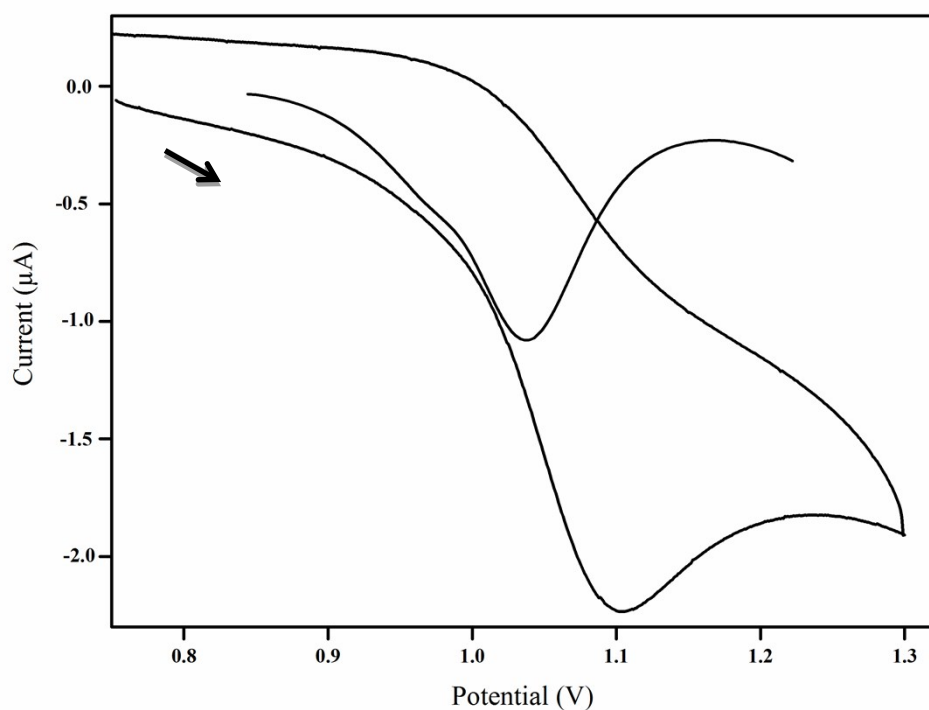


Figure S16: Cyclic voltammetry (CV) and differential pulse voltammetry (DPV) for $[\text{Fe}(\text{L1})(\text{SO}_3\text{CF}_3)]\text{SO}_3\text{CF}_3$, **1** (1×10^{-3} M) using TBAP (0.1 M) as supporting electrolyte in acetonitrile. $\text{Ag}(\text{s})/\text{Ag}^+$ (0.01 M, 0.10 M TBAP) as reference electrode. Platinum disc and platinum wire were used as working and counter electrodes respectively. Scan rate: 100 mVs^{-1} .

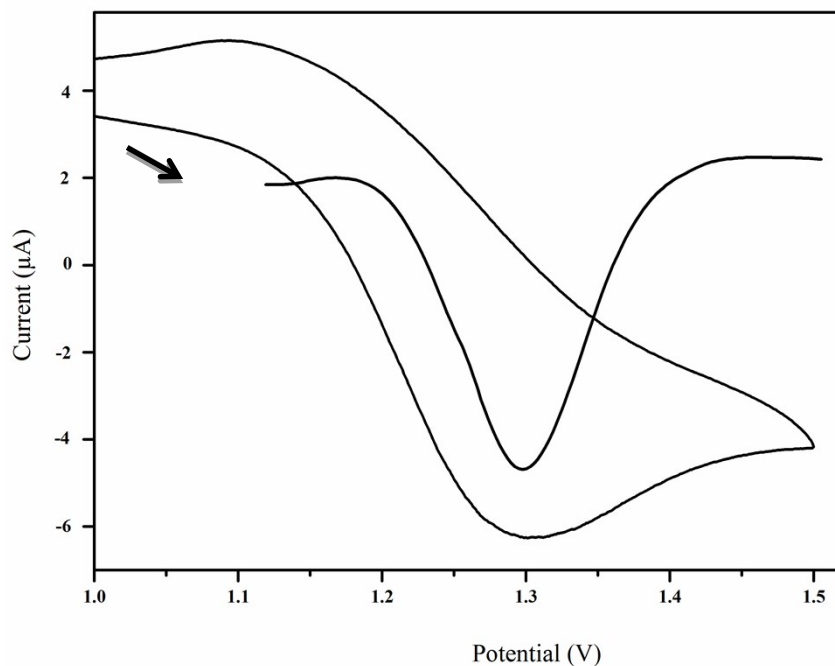


Figure S17. Cyclic voltammetry (CV) and differential pulse voltammetry (DPV) for $[\text{Fe}(\text{L}2)(\text{SO}_3\text{CF}_3)]\text{SO}_3\text{CF}_3$, **2** (1×10^{-3} M) using TBAP (0.1 M) as supporting electrolyte in acetonitrile. $\text{Ag}(\text{s})/\text{Ag}^+$ (0.01 M, 0.10 M TBAP) as reference electrode. Platinum disc and platinum wire were used as working and counter electrodes respectively. Scan rate: 100 mV s^{-1} .

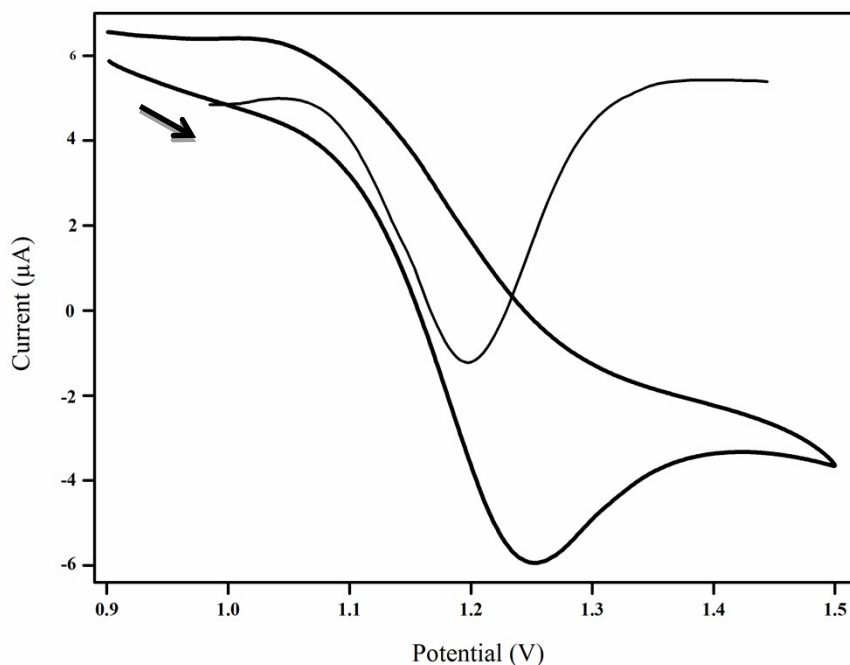


Figure S18. Cyclic voltammetry (CV) and differential pulse voltammetry for $[\text{Fe}(\text{L}3)(\text{SO}_3\text{CF}_3)]\text{SO}_3\text{CF}_3$, **3** (1×10^{-3} M) using TBAP (0.1 M) as supporting electrolyte in acetonitrile. $\text{Ag}(\text{s})/\text{Ag}^+$ (0.01 M, 0.10 M TBAP) as reference electrode. Platinum disc and platinum wire were used as working and counter electrodes respectively. Scan rate: 100 mV s^{-1} .

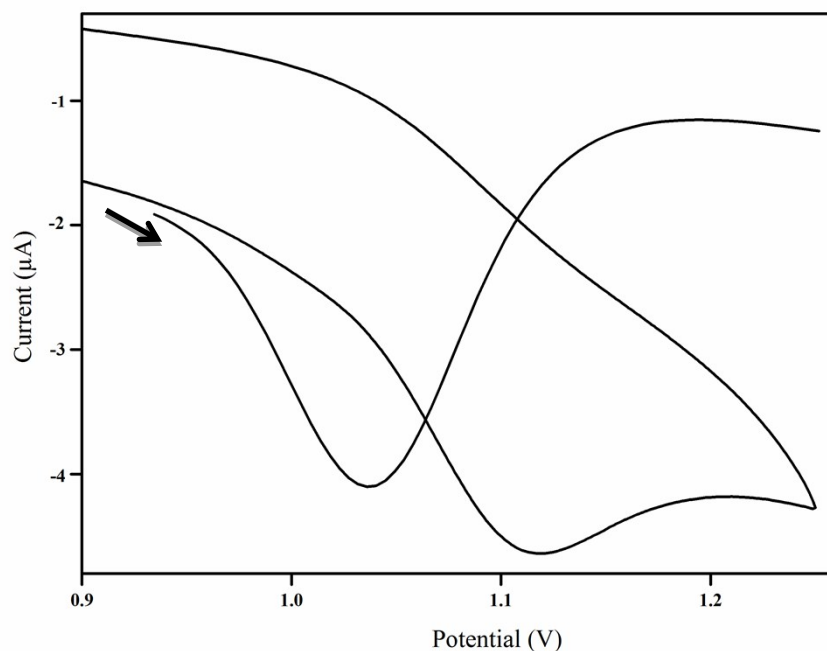


Figure S19. Cyclic voltammetry (CV) and differential pulse voltammetry for $[\text{Fe}(\text{L}1)(\text{acac}^{\text{Me}})]\text{SO}_3\text{CF}_3$, **1a** (1×10^{-3} M) using TBAP (0.1 M) as supporting electrolyte in acetonitrile. $\text{Ag}(\text{s})/\text{Ag}^+$ (0.01 M, 0.10 M TBAP) as reference electrode. Platinum disc and platinum wire were used as working and counter electrodes respectively. Scan rate: 100 mV s^{-1} .

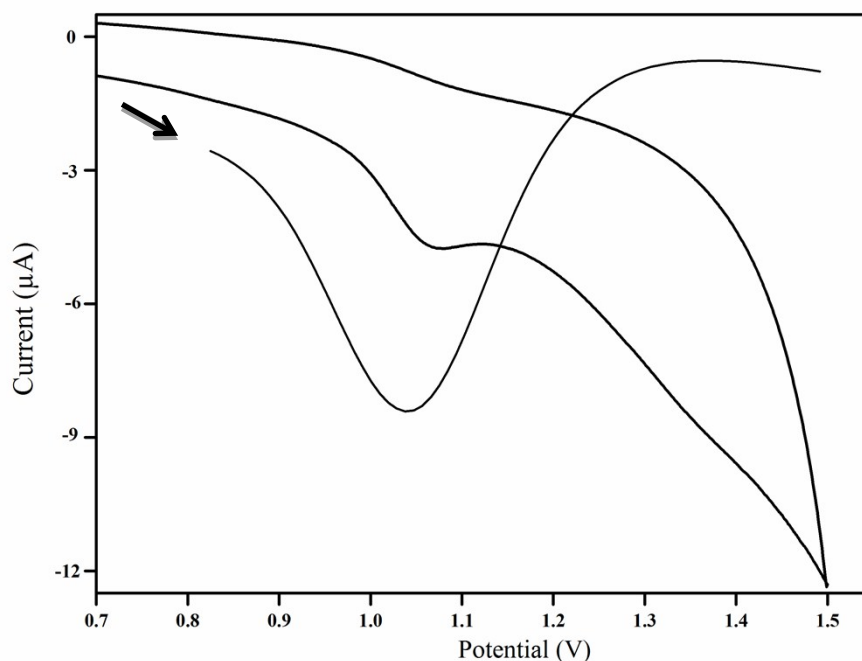


Figure S20. Cyclic voltammetry (CV) and differential pulse voltammetry (DPV) for $[\text{Fe}(\text{L}1)(\text{acac}^{\text{Ph}})]\text{SO}_3\text{CF}_3$, **1b** (1×10^{-3}) using TBAP (0.1 M) as supporting electrolyte in acetonitrile. $\text{Ag}(\text{s})/\text{Ag}^+$ (0.01 M, 0.10 M TBAP) as reference electrode. Platinum disc and platinum wire were used as working and counter electrodes respectively. Scan rate: 100 mV s^{-1} .

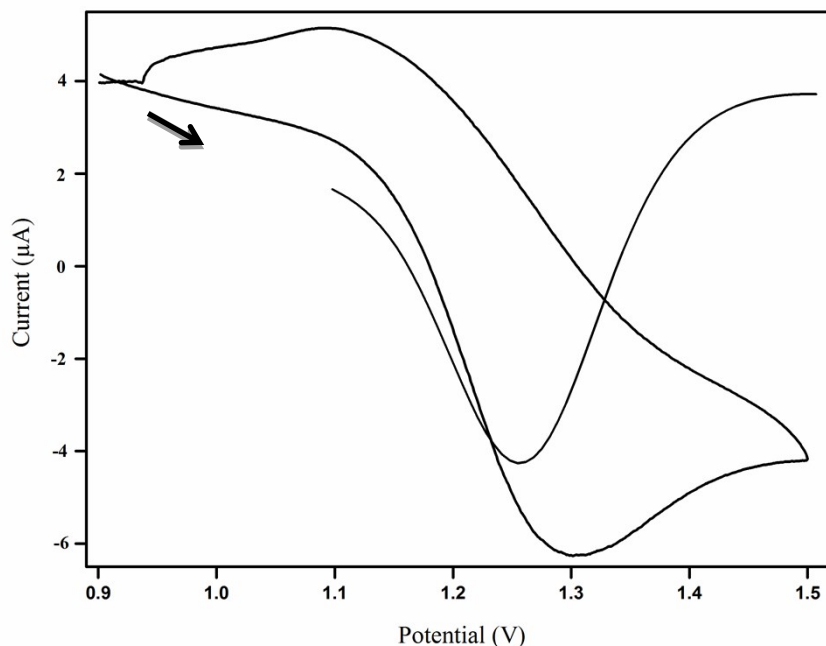


Figure S21. Cyclic voltammetry (CV) and differential pulse voltammetry for $[\text{Fe}(\text{L}2)(\text{acac}^{\text{Me}})]\text{SO}_3\text{CF}_3$, **2a** (1×10^{-3} M) using TBAP (0.1 M) as supporting electrolyte in acetonitrile. $\text{Ag}(\text{s})/\text{Ag}^+$ (0.01 M, 0.10 M TBAP) as reference electrode. Platinum disc and platinum wire were used as working and counter electrodes respectively. Scan rate: 100 mV s^{-1} .

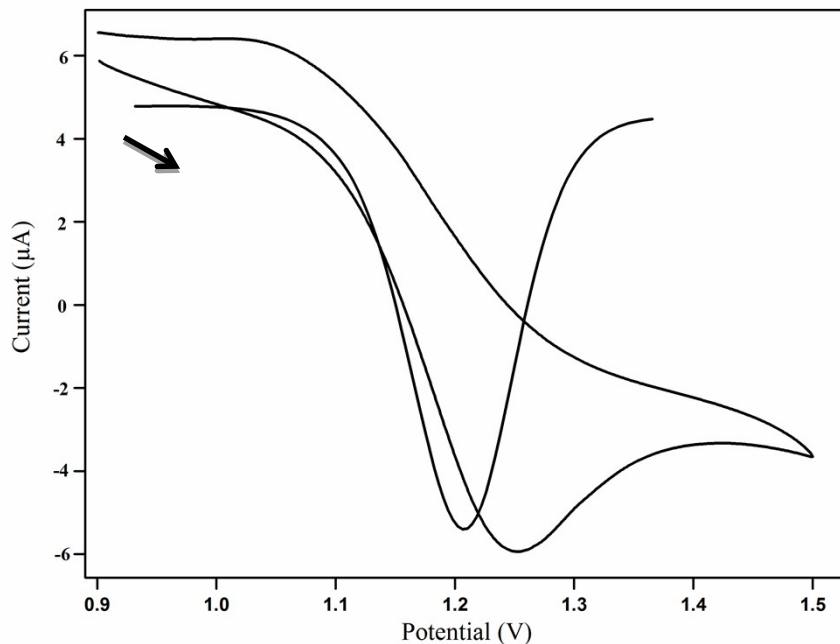


Figure S22. Cyclic voltammetry (CV) and differential pulse voltammetry for $[\text{Fe}(\text{L}3)(\text{acac}^{\text{Me}})]\text{SO}_3\text{CF}_3$, **3a** (1×10^{-3} M) using TBAP (0.1 M) as supporting electrolyte in acetonitrile. $\text{Ag}(\text{s})/\text{Ag}^+$ (0.01 M, 0.10 M TBAP) as reference electrode. Platinum disc and platinum wire were used as working and counter electrodes respectively. Scan rate: 100 mV s^{-1} .

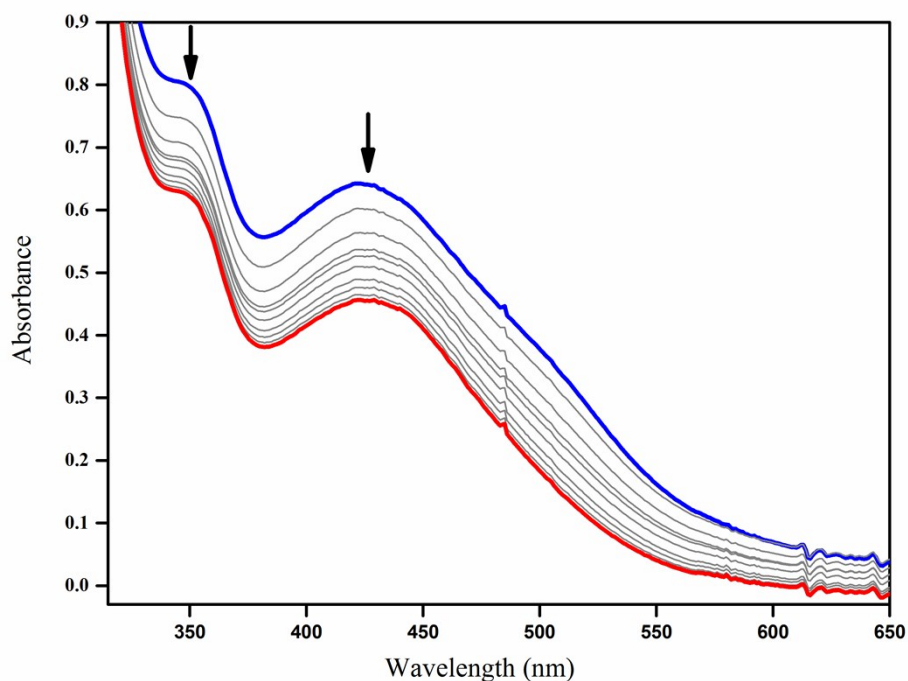


Figure S23. UV-Visible spectral changes for the reaction of **1a** (6×10^{-4} M) with saturated O_2 in acetonitrile/acetate buffer at 25°C . The monitored disappearance of Fe(II) to acac MLCT band at 430 nm with 120 seconds time interval.

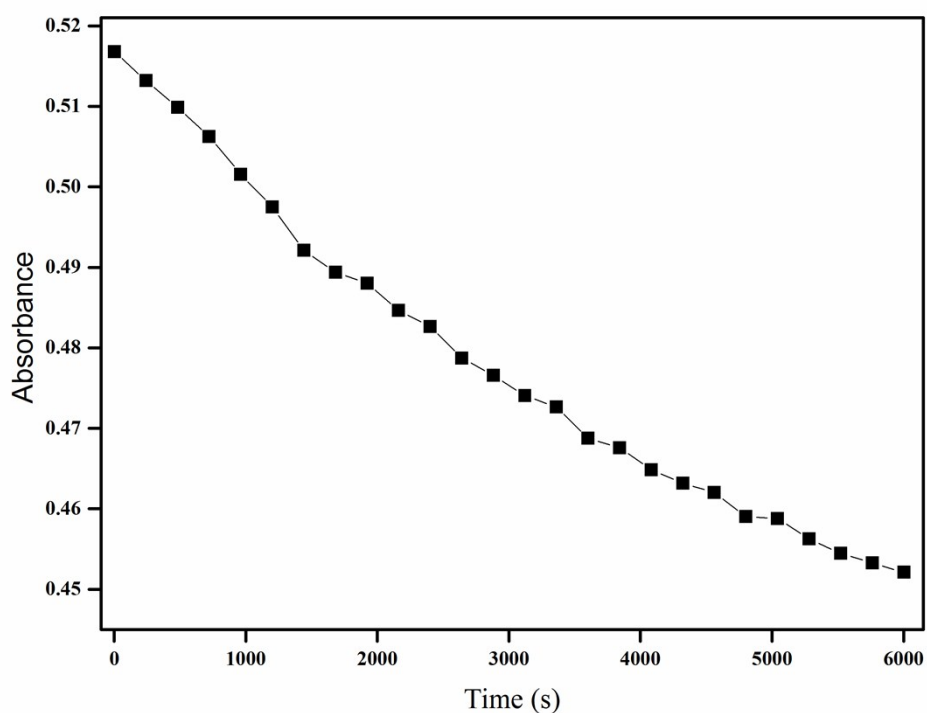


Figure S24. Plot of absorbance (430 nm) vs time the reaction of **1a** (6×10^{-4} M) with saturated O_2 in acetonitrile at 25°C .

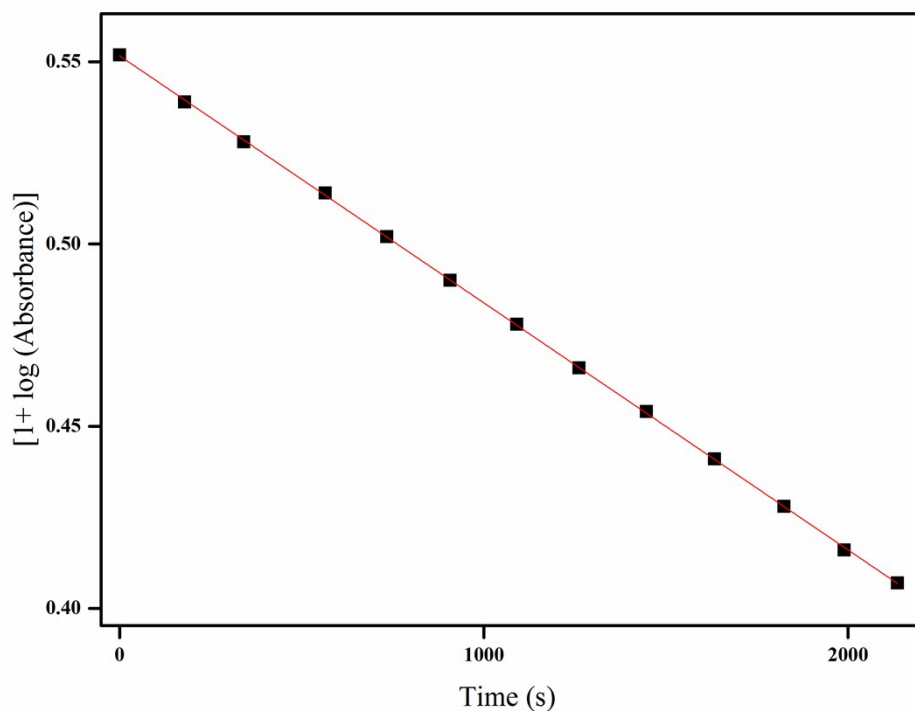


Figure S25. Plot of $[1 + \log(\text{Absorbance})]$ (430 nm) vs time the reaction of **1a** (6×10^{-4} M) with saturated O_2 in acetonitrile at 25°C .

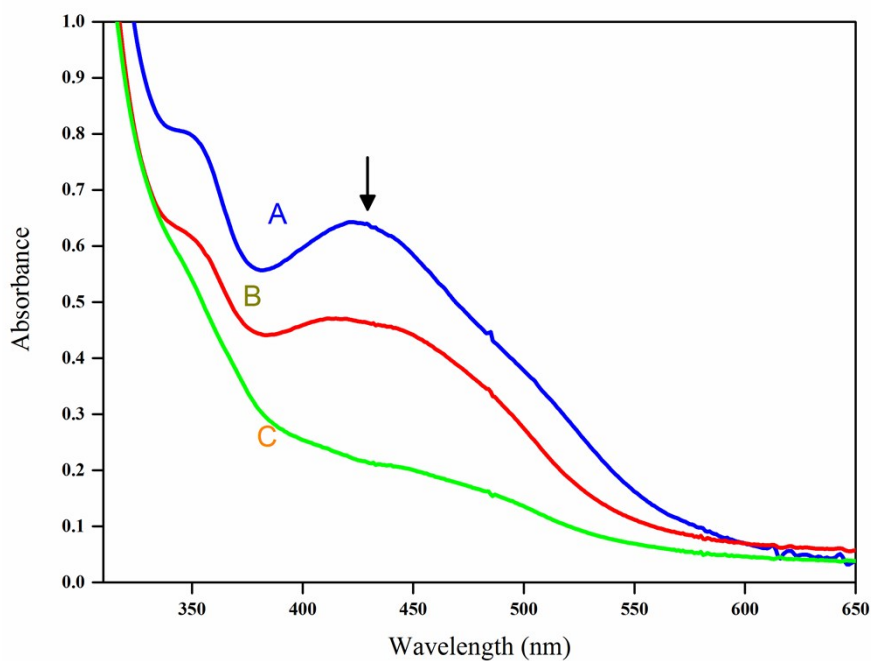


Figure S26. Comparison of MLCT band (430 nm) for the reaction of **1a** (6×10^{-4} M) with saturated O_2 and 0.5 equivalents of acetic acid at 25°C in acetonitrile/acetate buffer. Initial spectra (A), after 1800 s (B) and 6000 s (C).

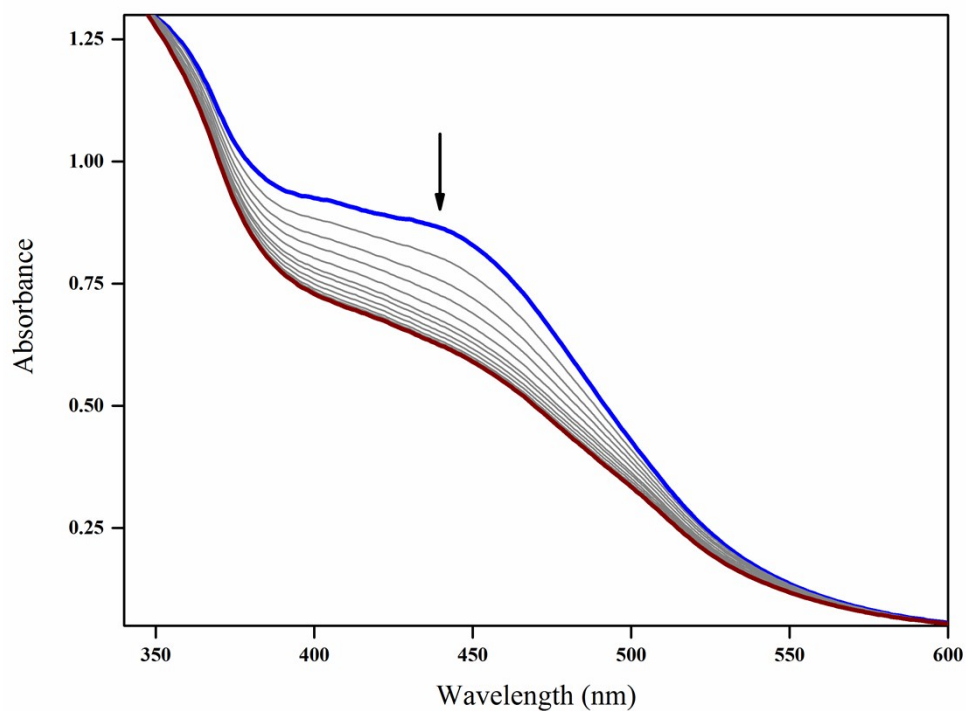


Figure S27. UV-Visible spectral changes for the reaction of **2a** (6×10^{-4} M) with saturated O_2 in acetonitrile/acetate buffer at $25^\circ C$. The monitored disappearance of Fe(II) to acac MLCT band at 440 nm with 180 seconds time interval.

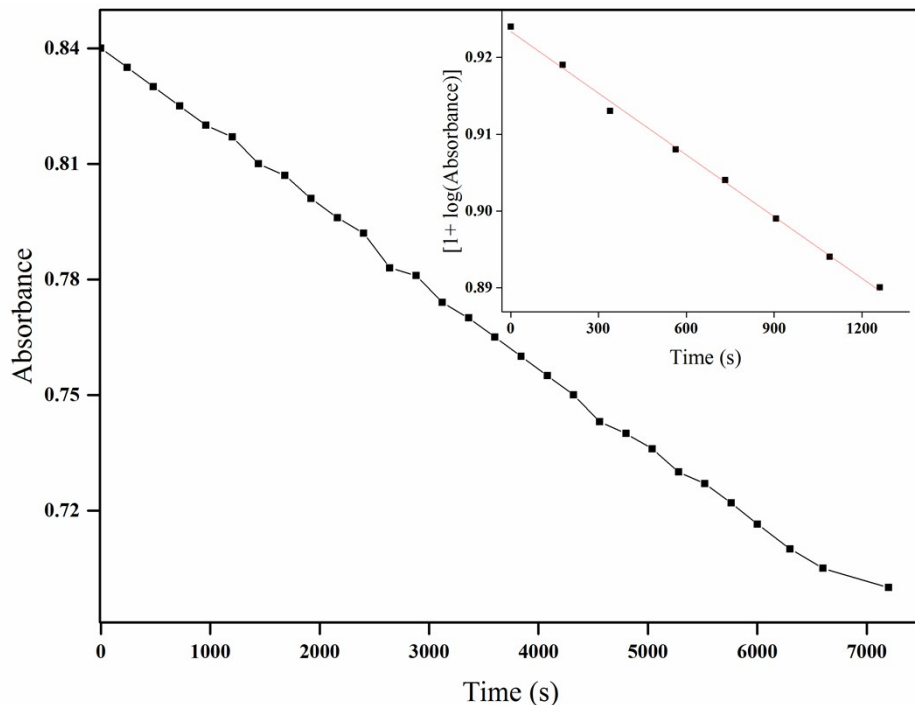


Figure S28. Plot of absorbance vs time for the reaction of **2a** (6×10^{-4} M) in acetonitrile with saturated O_2 at $25^\circ C$. Inset: Plot of $[1 + \log(\text{Absorbance})]$ (440 nm) vs time.

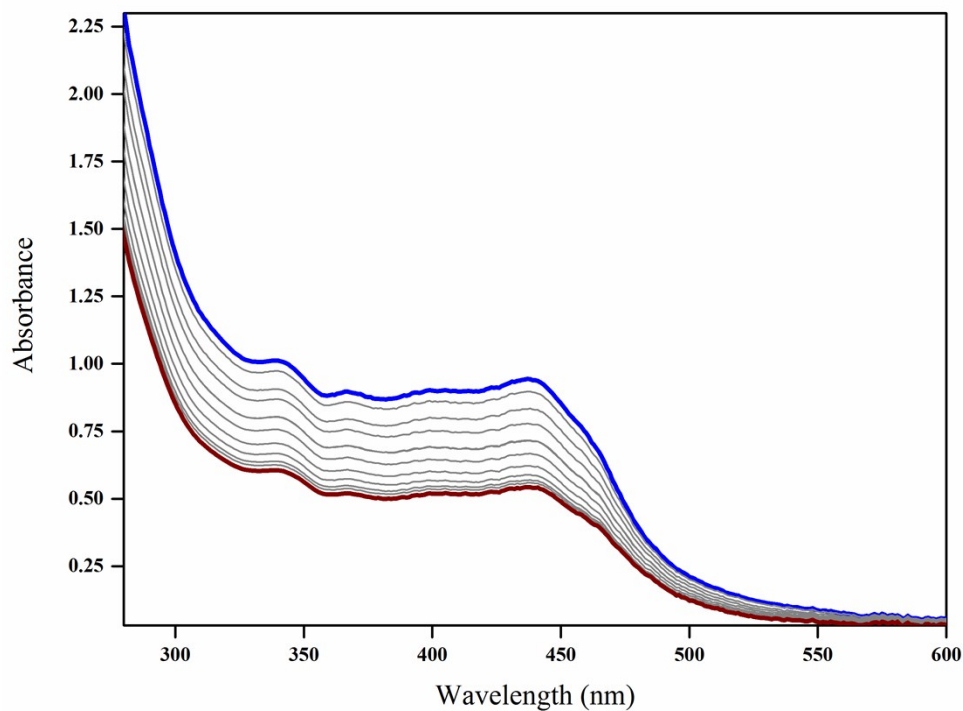


Figure S29. UV-Visible spectral changes for the reaction of **3a** (6×10^{-4} M) with saturated O_2 and 0.5 equivalents of acetic acid at $25^\circ C$ in acetonitrile/acetate buffer. The monitored disappearance of Fe(II) to acac MLCT band at 430 nm with 90 seconds time interval.

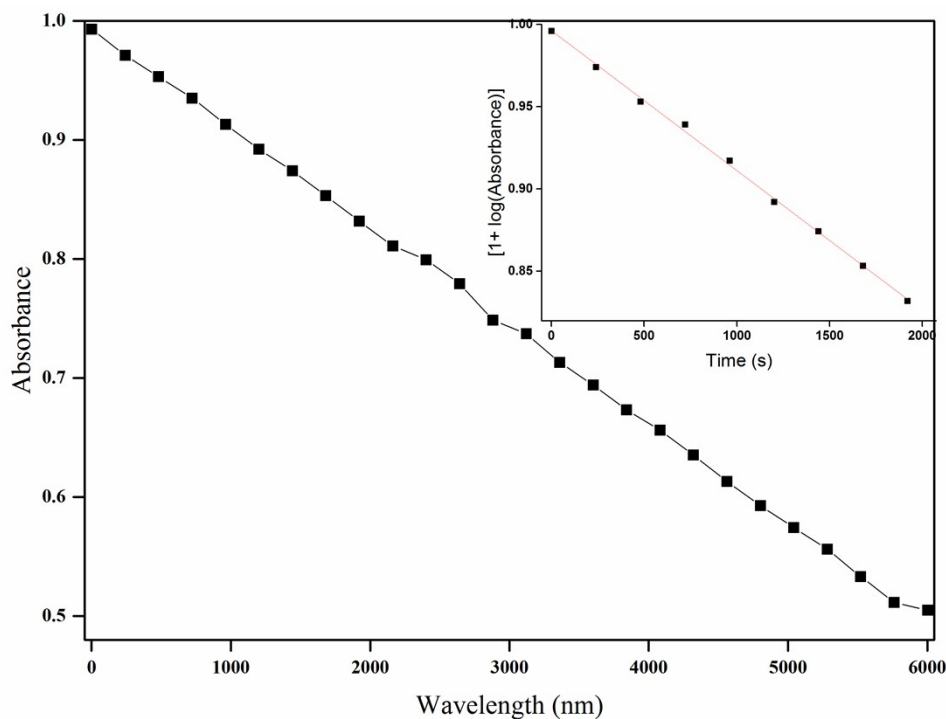


Figure S30. Plot of absorbance (430 nm) vs time for the reaction of **3a** (6×10^{-4} M) with saturated O_2 in acetonitrile and 0.5 equivalents of acetic acid at $25^\circ C$. Inset: Plot of $[1 + \log(\text{Absorbance})]$ (430 nm) vs time.

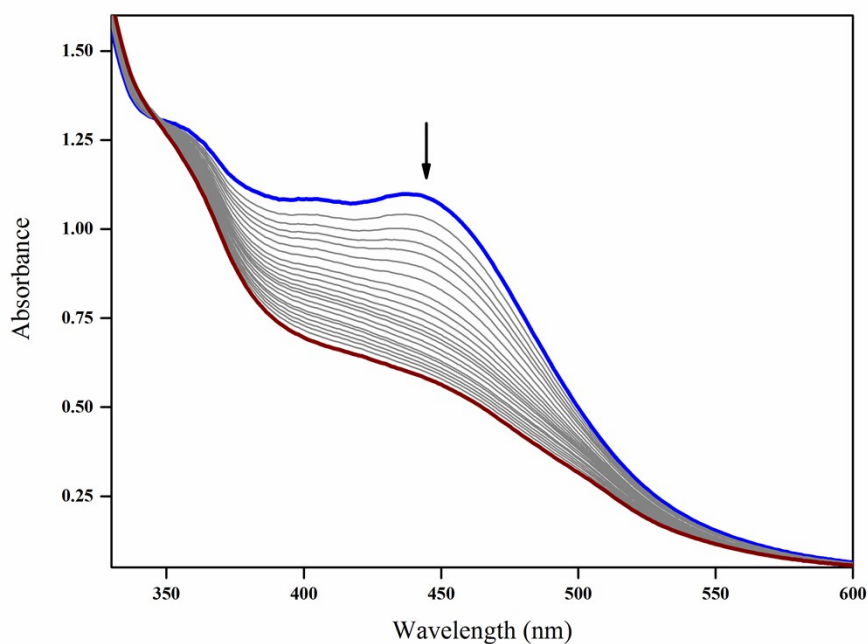


Figure S31. UV-Visible spectral changes for the reaction of **2a** (6×10^{-4} M) with saturated O_2 and 0.5 equivalents of acetic acid at $25^\circ C$ in acetonitrile\acetate buffer . The monitored disappearance of Fe(II) to acac MLCT band at 440 nm with 30 seconds time interval.

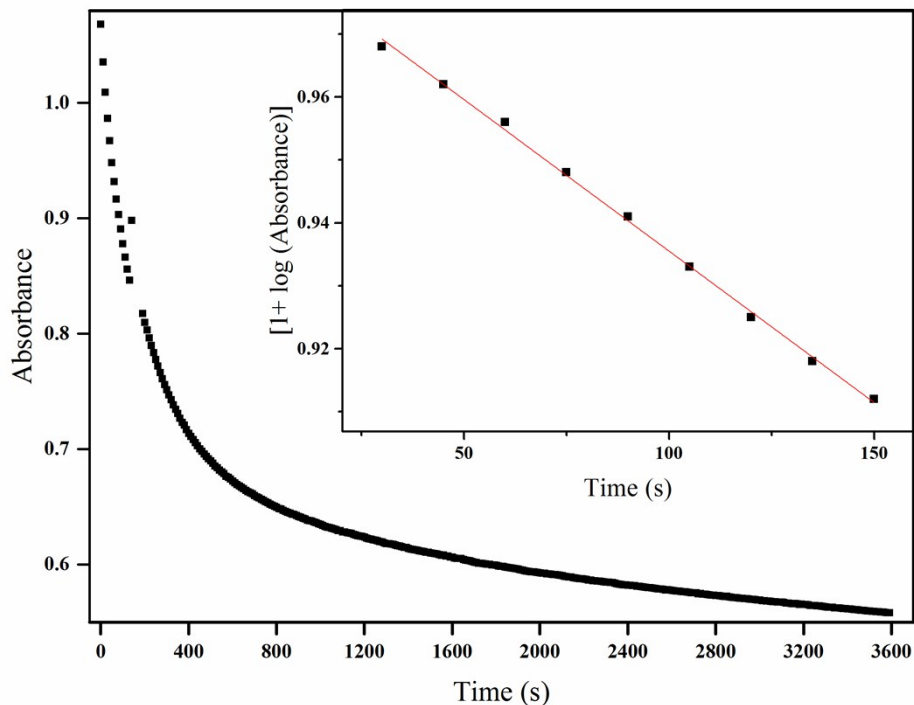


Figure S32. Plot of absorbance (440 nm) vs time for the reaction of **2a** (6×10^{-4} M) in acetonitrile with saturated O_2 and 0.5 equivalents of acetic acid at $25^\circ C$. Inset: Plot of $[1 + \log(\text{Absorbance})]$ vs time.

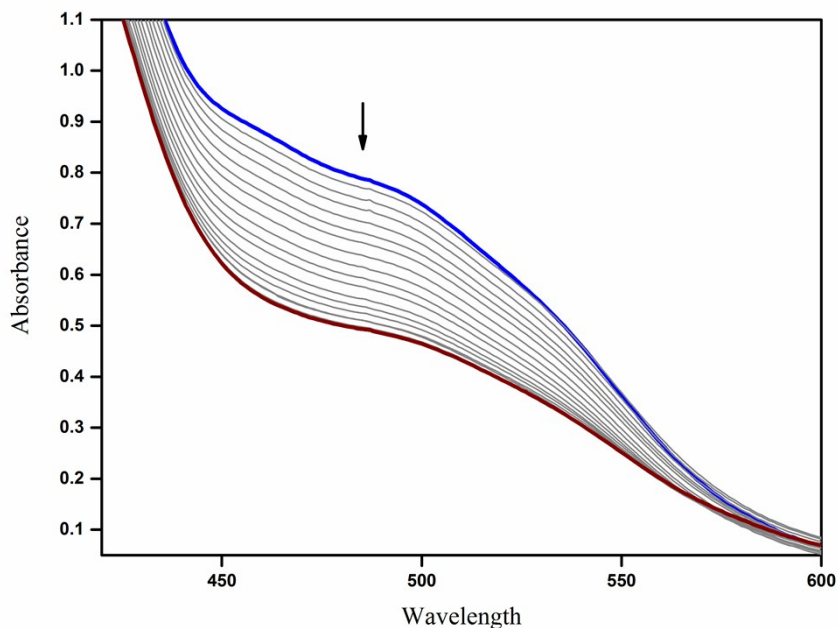


Figure S33. UV-Visible spectral changes for the reaction of **1b** (6×10^{-4} M) with saturated O_2 and 0.5 equivalents acetic acid at $25^\circ C$ in acetonitrile/acetate buffer. The monitored disappearance of Fe(II) to acac MLCT band at 490 nm with 30 seconds time interval.

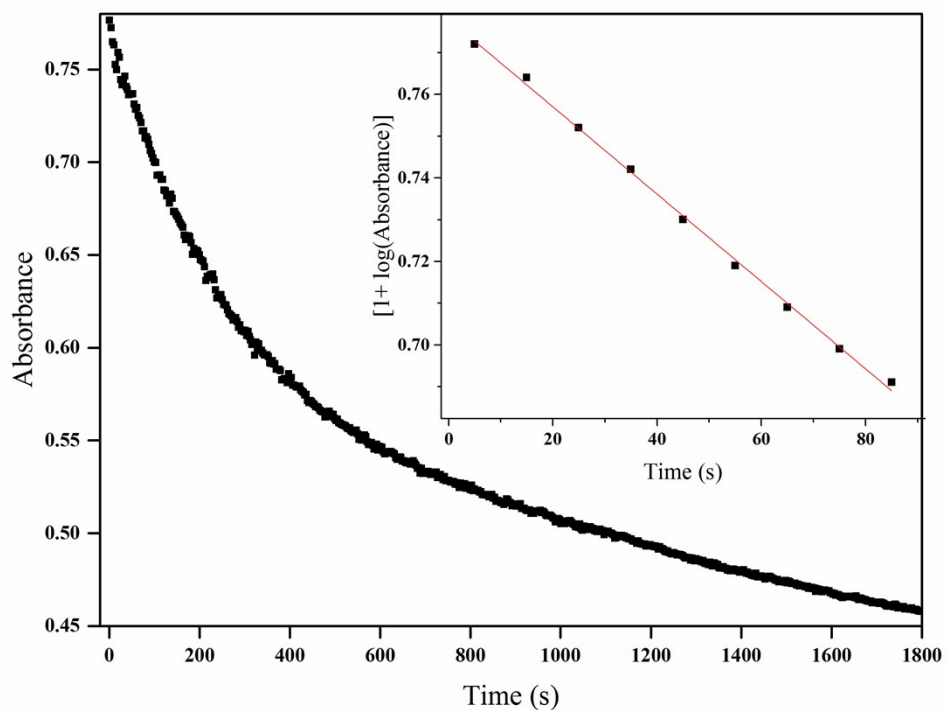


Figure S34. Plot of absorbance (490 nm) vs time for the reaction of **1b** (6×10^{-4} M) with saturated O_2 and 0.5 equivalents acetic acid in acetonitrile at $25^\circ C$. Inset: Plot of $[1 + \log(\text{Absorbance})]$ vs time.

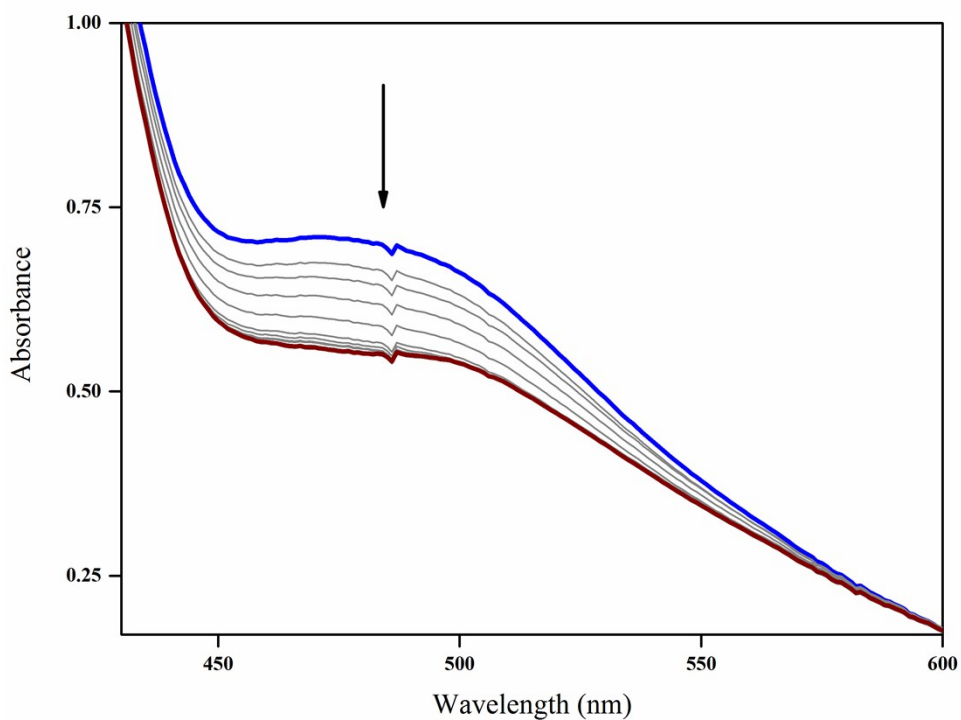


Figure S35. UV- Visible spectral changes for the reaction of **2b** (6×10^{-4} M) with saturated O_2 and 0.5 equivalents acetic acid at $25^\circ C$ in acetonitrile\acetate buffer. The monitored disappearance of Fe(II) to acac MLCT band at 485 nm with 30 seconds time interval.

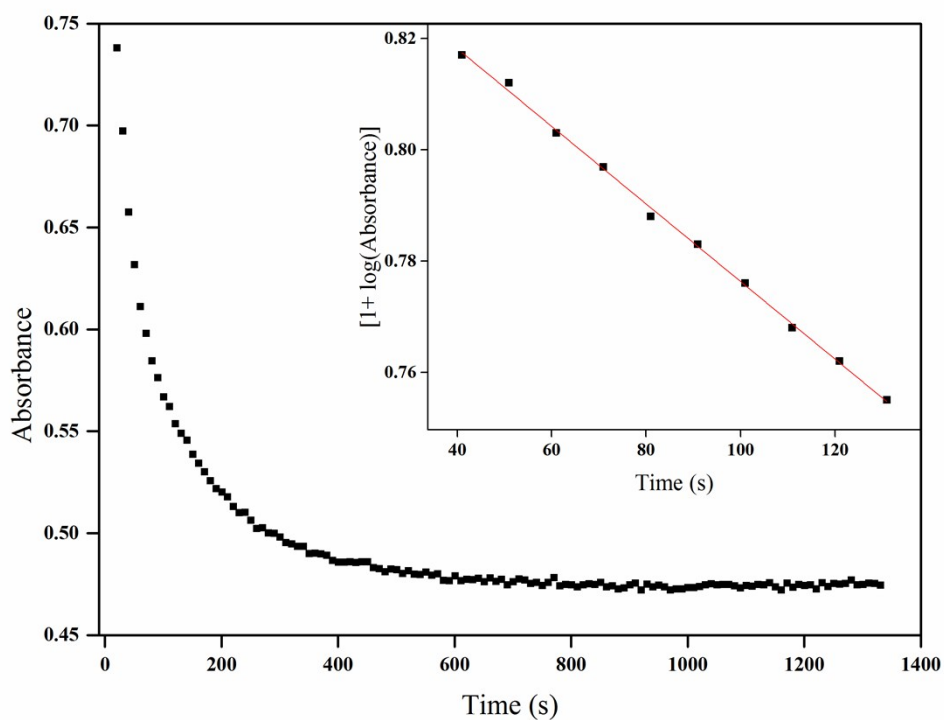


Figure S36. Plot of absorbance (485 nm) vs time for the reaction of **2b** (6×10^{-4} M) with saturated O_2 and 0.5 equivalents acetic acid in acetonitrile at $25^\circ C$. Inset: Plot of $[1 + \log(\text{Absorbance})]$ vs time

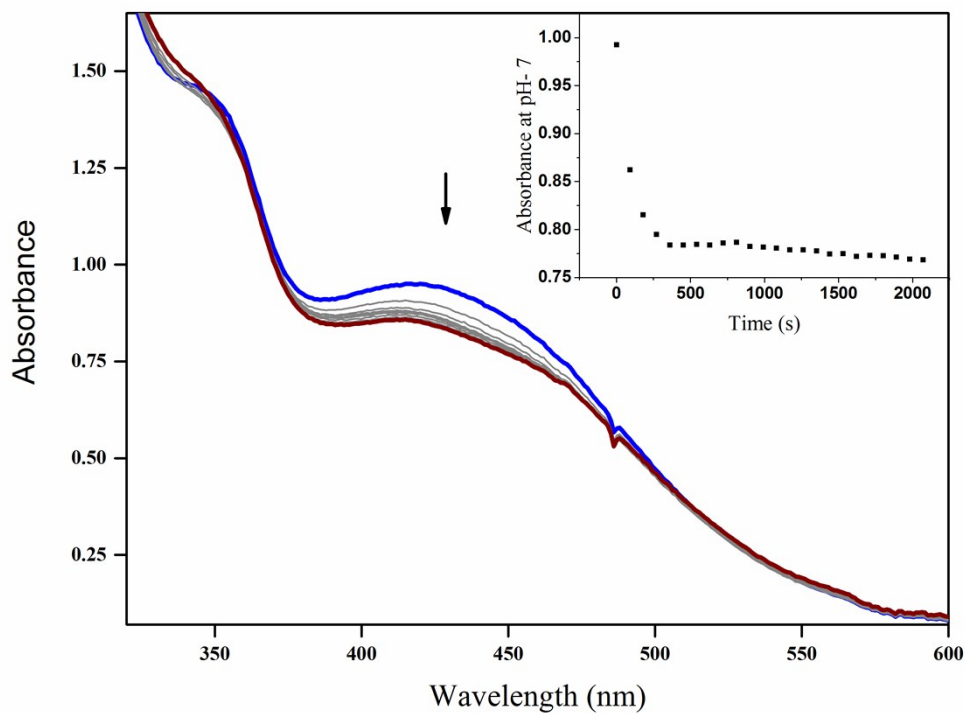


Figure S37. The UV- Visible spectral changes for the reaction of **1a** (6×10^{-4} M) with saturated O_2 in acetonitrile/acetate buffer at pH 7.0 at $25^\circ C$ in acetonitrile/acetate buffer . Inset: Absorbance (430 nm) vs time.

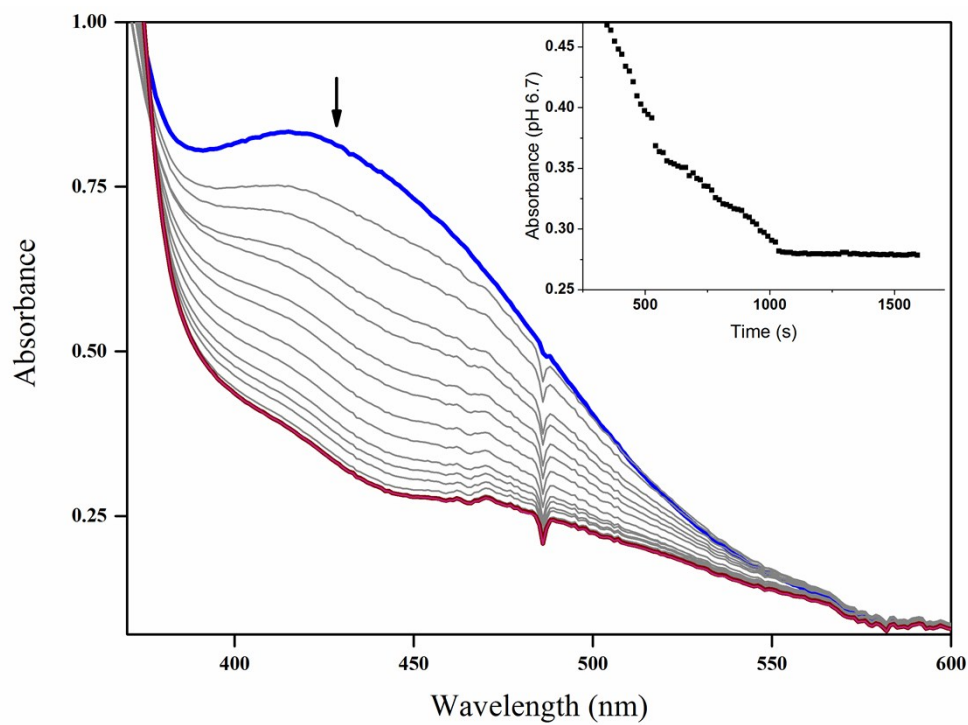


Figure S38. The UV- Visible spectral changes for the reaction of **1a** (6×10^{-4} M) with saturated O_2 in acetonitrile in acetonitrile/acetate buffer at pH 6.7 at $25^\circ C$. Inset: Absorbance (430 nm) vs time.

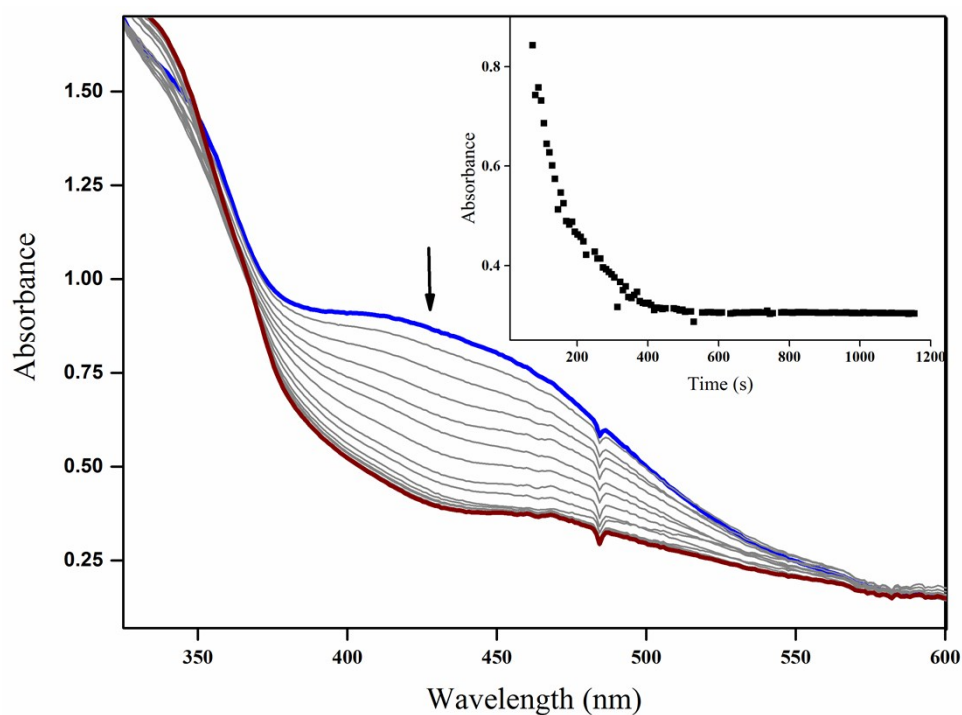


Figure S39. The UV- Visible spectral changes for the reaction of **1a** (6×10^{-4} M) with saturated O_2 in acetonitrile/acetate buffer at pH 6.3 at $25^\circ C$. Inset: Absorbance (430 nm) vs time.

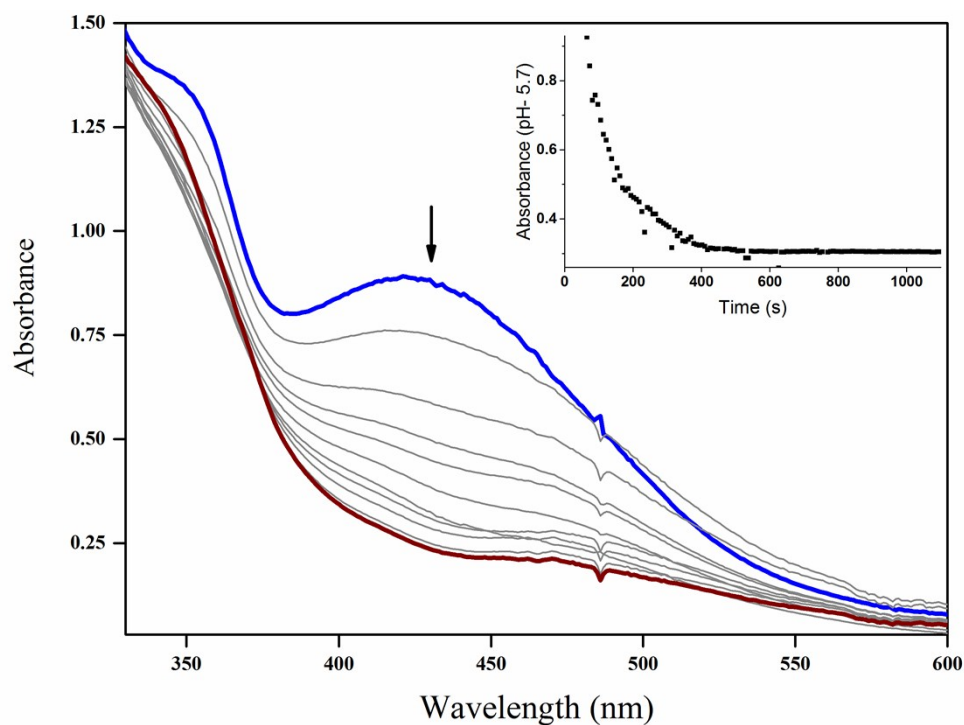


Figure S40. The UV- Visible spectral changes for the reaction of **1a** (6×10^{-4} M) with saturated O_2 in acetonitrile/acetate buffer at pH 5.7 at $25^\circ C$. Inset: Absorbance (430 nm) vs time.

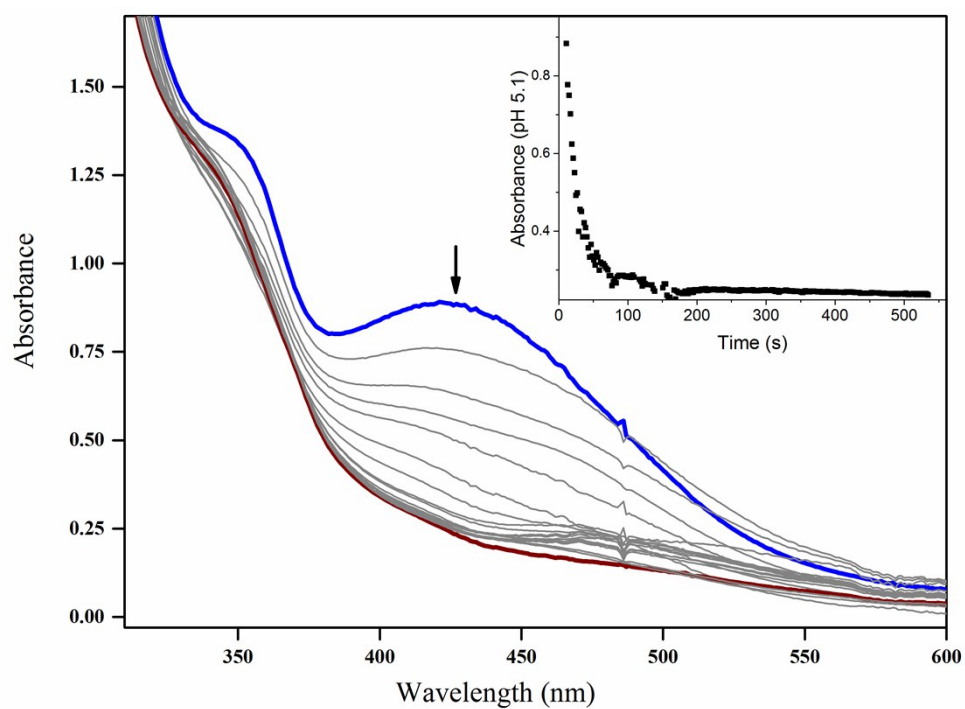


Figure S41. The UV-Visible spectral changes for the reaction of **1a** (6×10^{-4} M) with saturated O_2 in acetonitrile/acetate buffer at pH 5.1 at $25^\circ C$. Inset: Absorbance (430 nm) vs time.

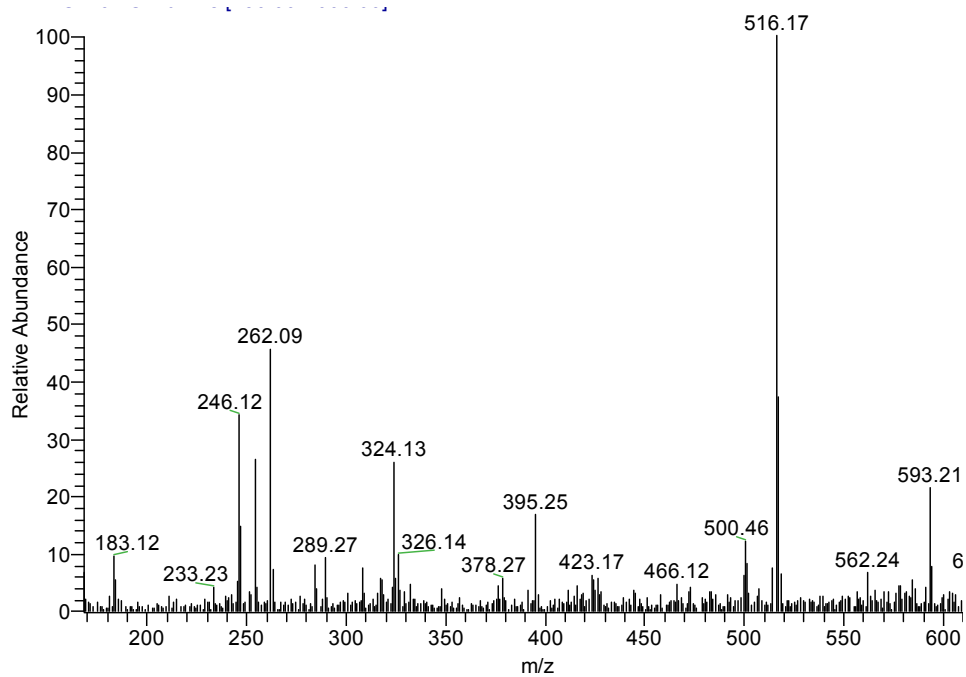
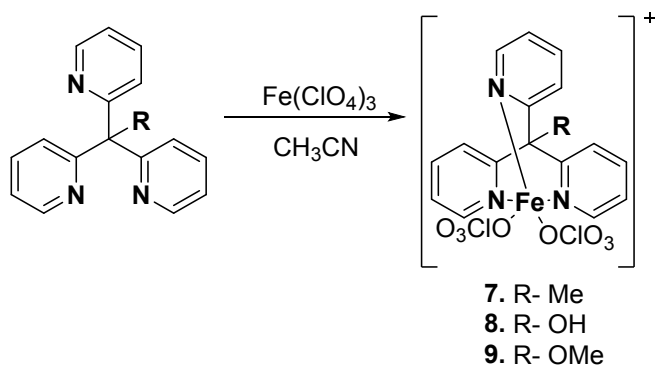


Figure S42. The ESI MS for complex $[\text{Fe}(\text{L1})(\text{ClO}_4)_2]\text{ClO}_4$ **7** in acetonitrile.

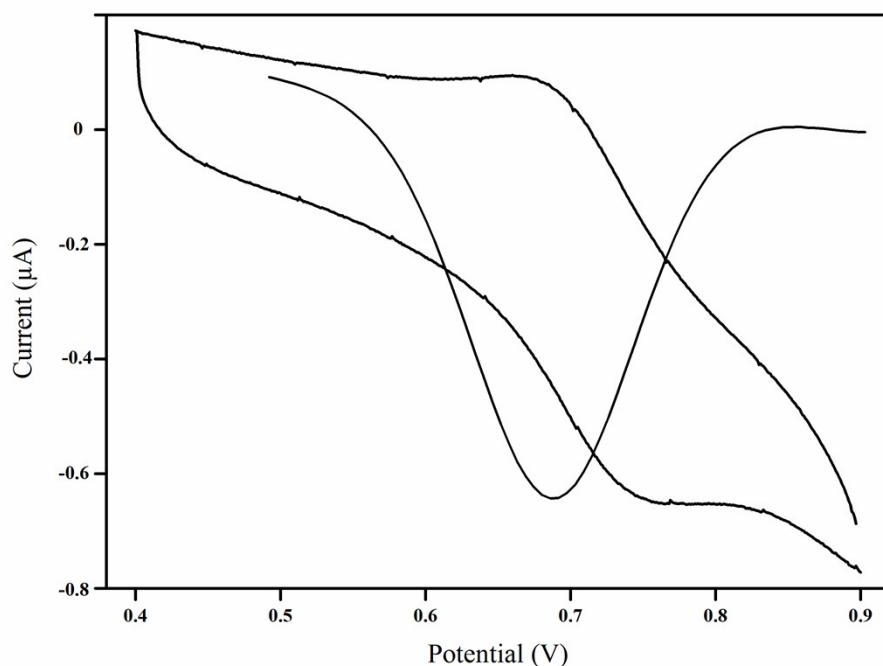


Figure S43. Cyclic voltammetry and differential pulse voltammetry of $\text{Fe(L1)(ClO}_4)_2\text{ClO}_4$, **7** (1×10^{-3} M) using TBAP (0.1 M) as supporting electrolyte in acetonitrile. Ag(s)/Ag^+ (0.01 M, 0.10 M TBAP) as reference electrode; 0.681 V to convert to NHE. Platinum disc and platinum wire were used as working and counter electrodes respectively.

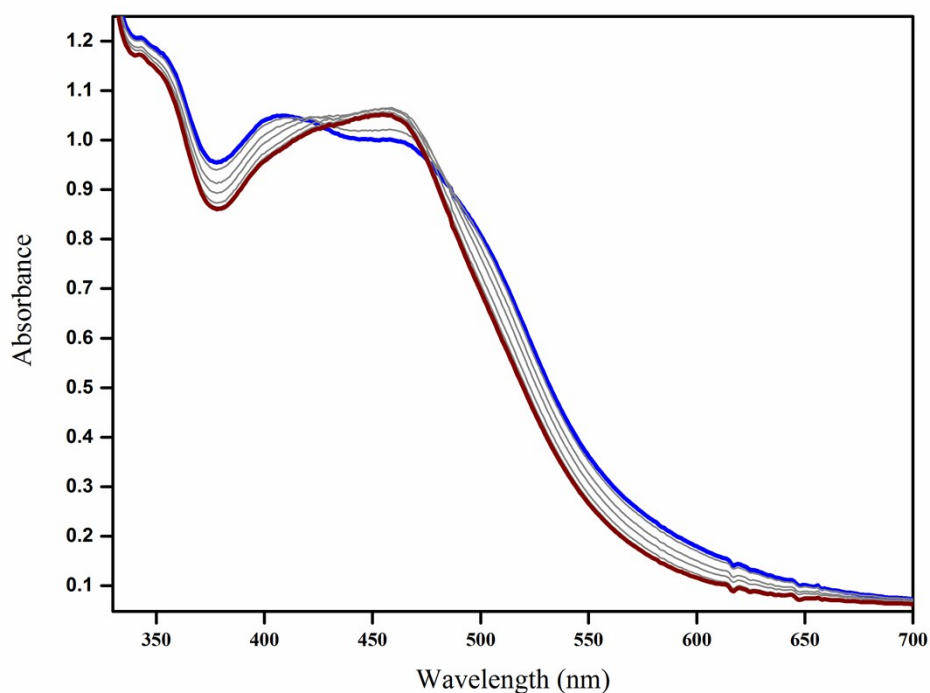


Figure S44. UV-Visible spectral changes for the reaction of adduct (6×10^{-4} M) generated from $[\text{Fe(L1)(ClO}_4)_2]\text{ClO}_4$, **7** and $\text{Na(acac)}_{\text{Me}}$ (6×10^{-4} M) with saturated O_2 in acetonitrile and 0.5 equivalents of acetic acid.

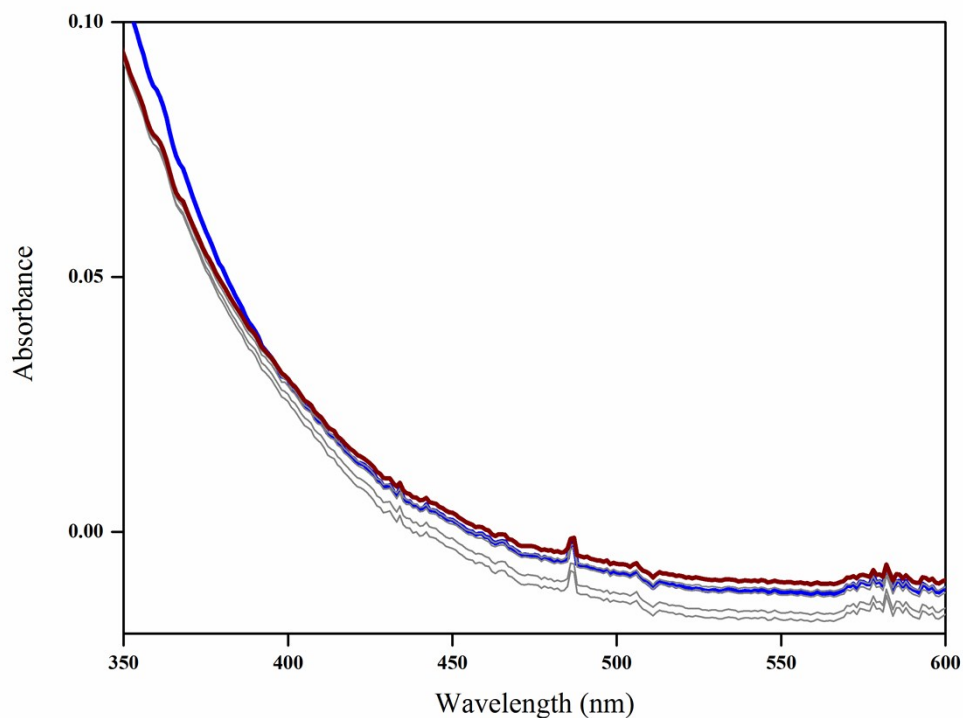


Figure S45. The UV-Visible spectral changes for the reaction of $[\text{Zn}(\text{L1})(\text{ClO}_4)_2]$ ($6 \times 10^{-4} \text{ M}$) and $\text{Na}(\text{acac})_{\text{Me}}$ ($6 \times 10^{-4} \text{ M}$) with saturated O_2 in acetonitrile in presence of 0.5 equivalent of acetic acid.

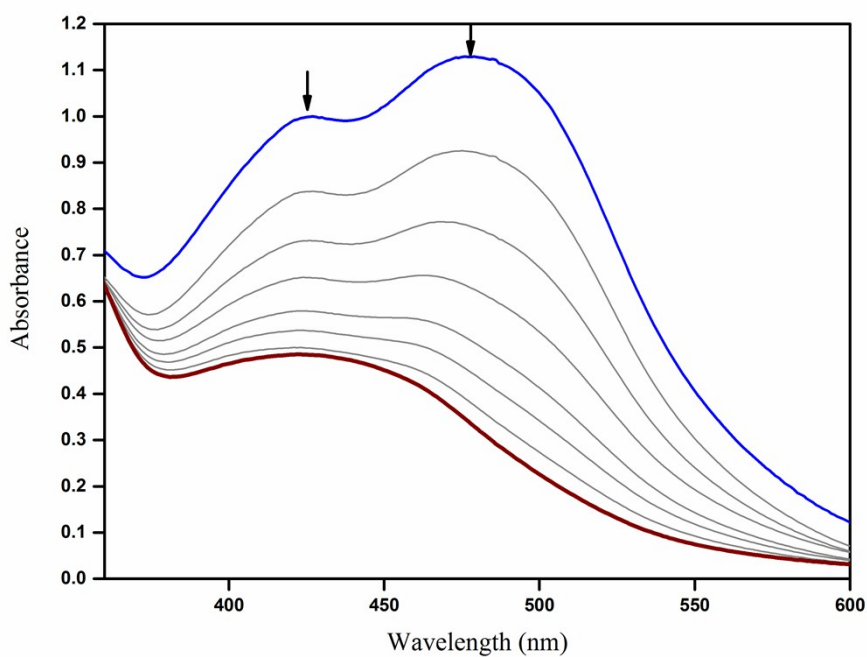


Figure S46. UV-Visible spectral changes for the reaction of **2a** ($6 \times 10^{-4} \text{ M}$) with ten equivalents of *tert*-butyl hydroperoxide and 0.5 equivalents of acetic acid at 25°C in acetonitrile/acetate buffer. The monitored disappearance of Fe(II) to acac MLCT band at 440 nm with 45 seconds time interval.

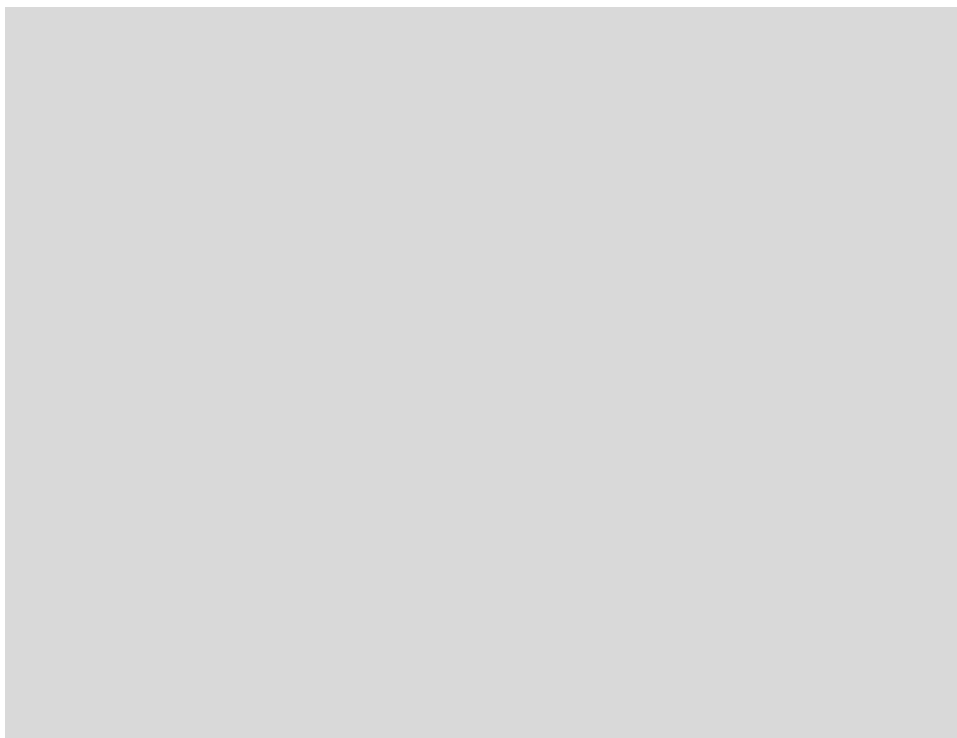


Figure S47. Plot of absorbance (440 nm) vs time for the reaction of **2a** (6×10^{-4} M) with 10 equivalents of *tert*-butyl hydroperoxide and 0.5 equivalents of acetic acid in acetonitrile at 25°C. Inset: Plot of $[1 + \log(\text{Absorbance})]$ vs time.

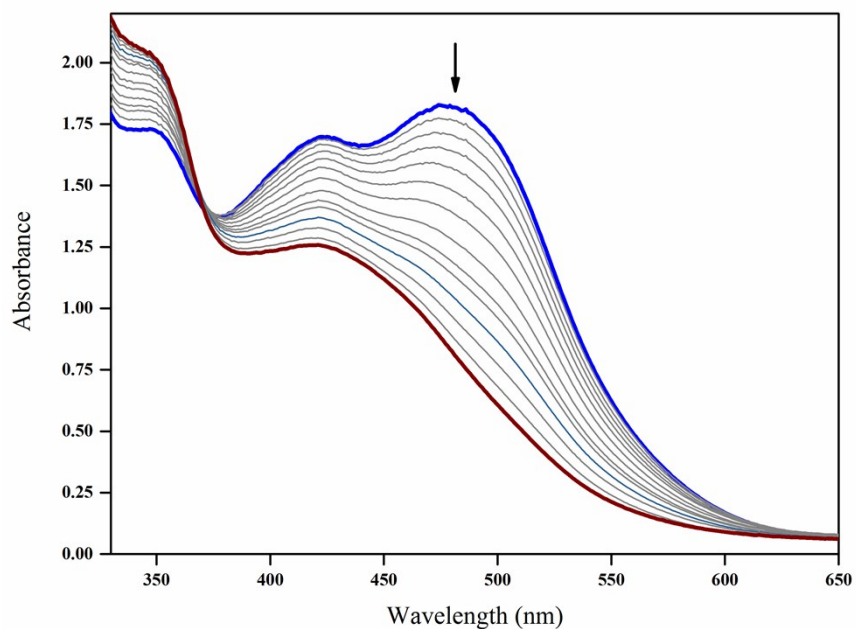


Figure S48. UV-Visible spectral changes for the reaction of **3a** (6×10^{-4} M) with ten equivalents of *tert*-butyl hydroperoxide and 0.5 equivalents of acetic acid at 25°C in acetonitrile/acetate buffer. The monitored disappearance of Fe(II) to acac MLCT band at 430 nm with 30 seconds time interval.

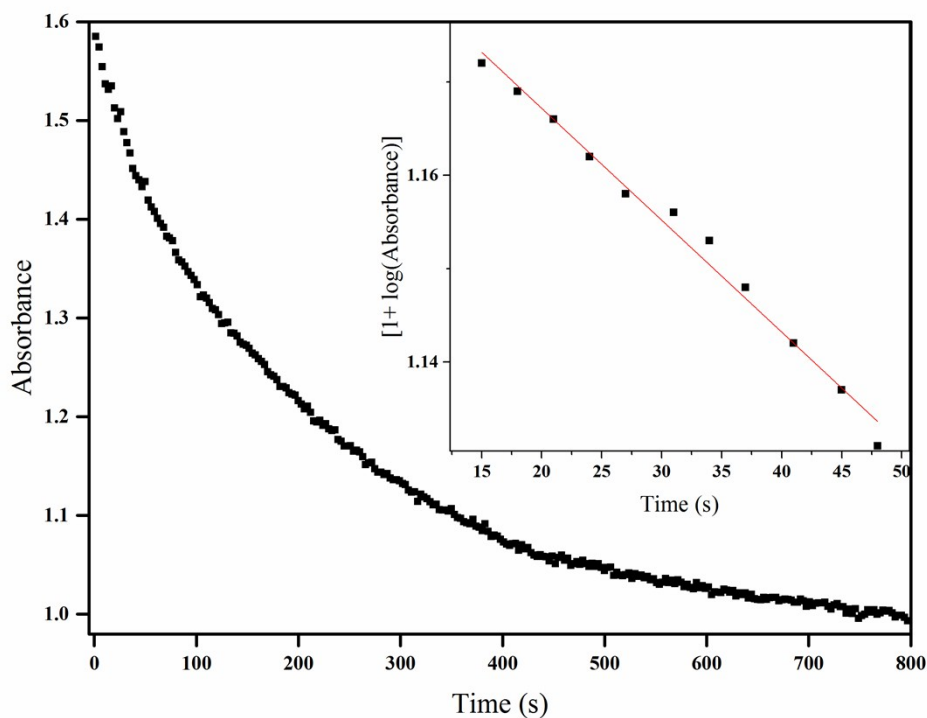


Figure S49. Plot of absorbance (430 nm) vs time for the reaction of **3a** (6×10^{-4} M) with 10 equivalents of *tert*-butyl hydroperoxide and 0.5 equivalents of acetic acid in acetonitrile at 25°C. Inset: Plot of $[1 + \log(\text{Absorbance})]$ vs time.

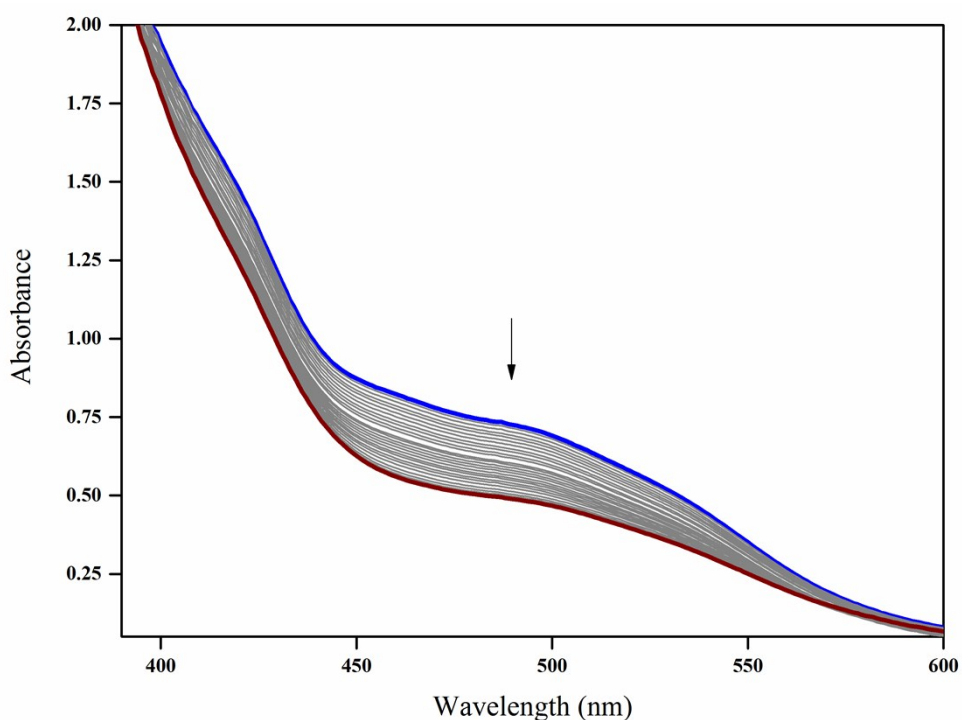


Figure S50. UV-Visible spectral changes for the reaction of **1b** (6×10^{-4} M) with 10 equivalents of *tert*-butyl hydroperoxide and 0.5 equivalents of acetic acid at 25°C in acetonitrile\acetate buffer. The monitored disappearance of Fe(II) to acac MLCT band at 490 nm with 15 seconds time interval.

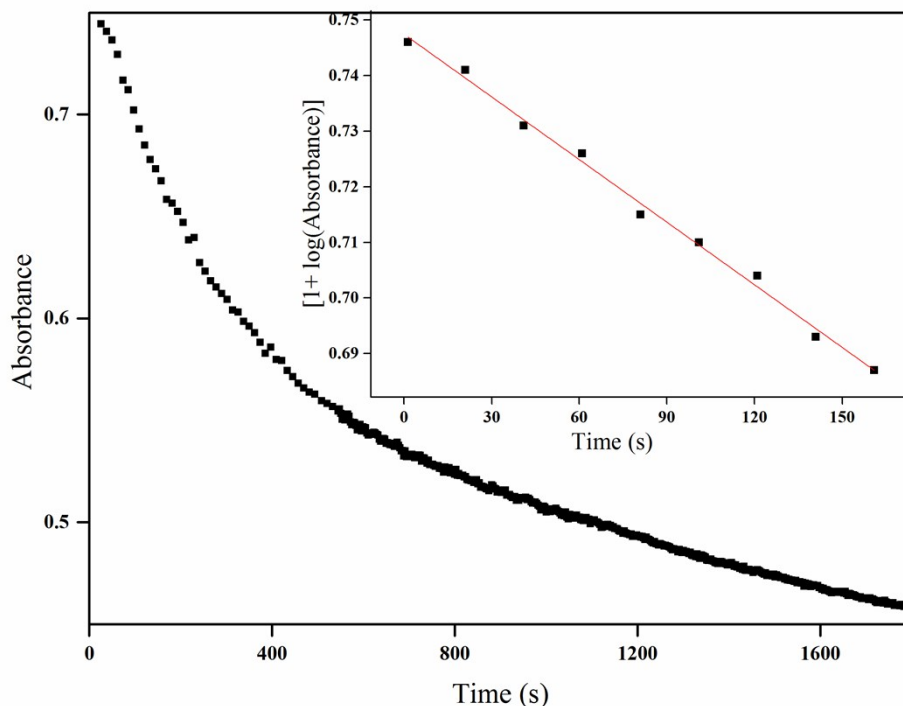


Figure S51. Plot of absorbance (490 nm) vs time for the reaction of **1b** (6×10^{-4} M) with ten equivalents of *tert*-butyl hydroperoxide and 0.5 equivalents of acetic acid in acetonitrile at 25°C. Inset: Plot of $[1 + \log(\text{Absorbance})]$ vs time.

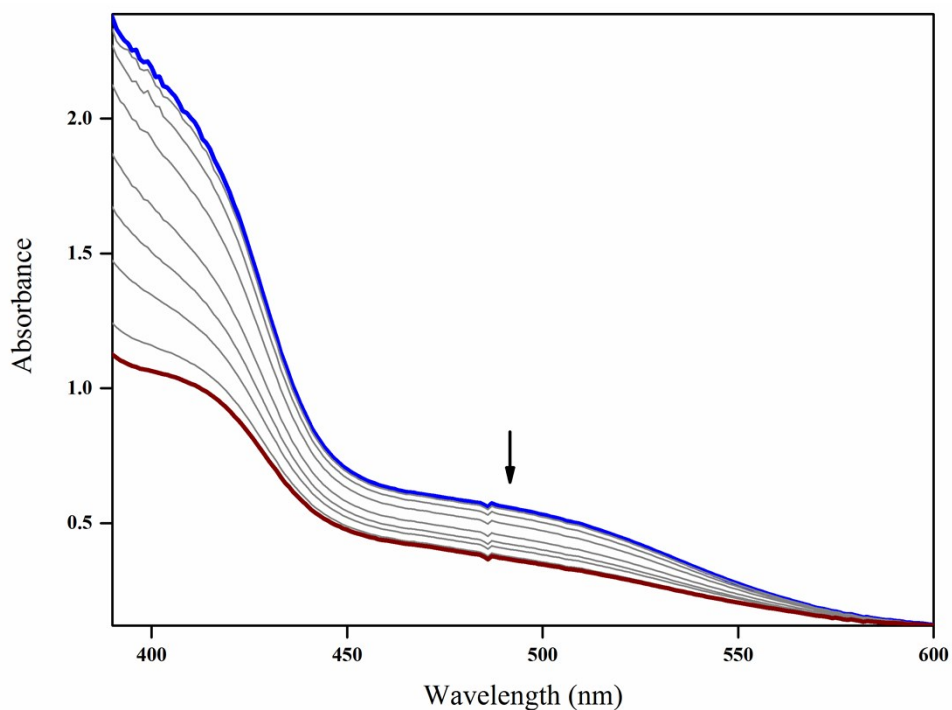


Figure S52. UV-Visible spectral changes for the reaction of **2b** (6×10^{-4} M) with ten equivalents of *tert*-butyl hydroperoxide and 0.5 equivalents of acetic acid at 25°C in acetonitrile/acetate buffer. The monitored disappearance of Fe(II) to acac MLCT band at 485 nm with 30 seconds time interval.

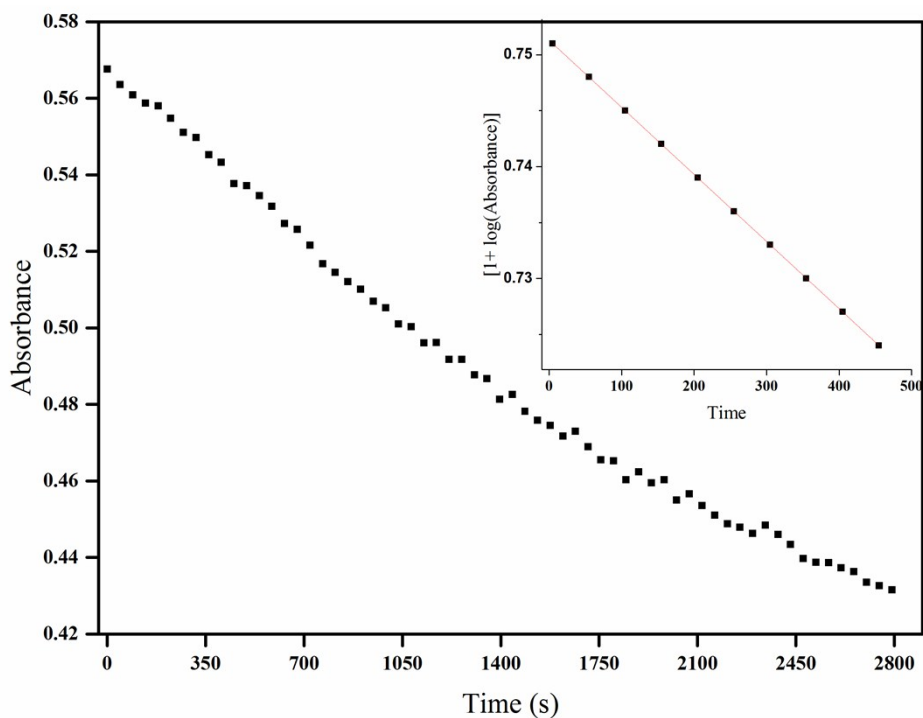


Figure S53. Plot of absorbance vs time for the reaction of **2b** (6×10^{-4} M) with ten equivalents of *tert*-butyl hydroperoxide and 0.5 equivalents of acetic acid in acetonitrile at 25°C in acetonitrile\acetate buffer . Inset: Plot of $[1 + \log(\text{Absorbance})]$ vs time.

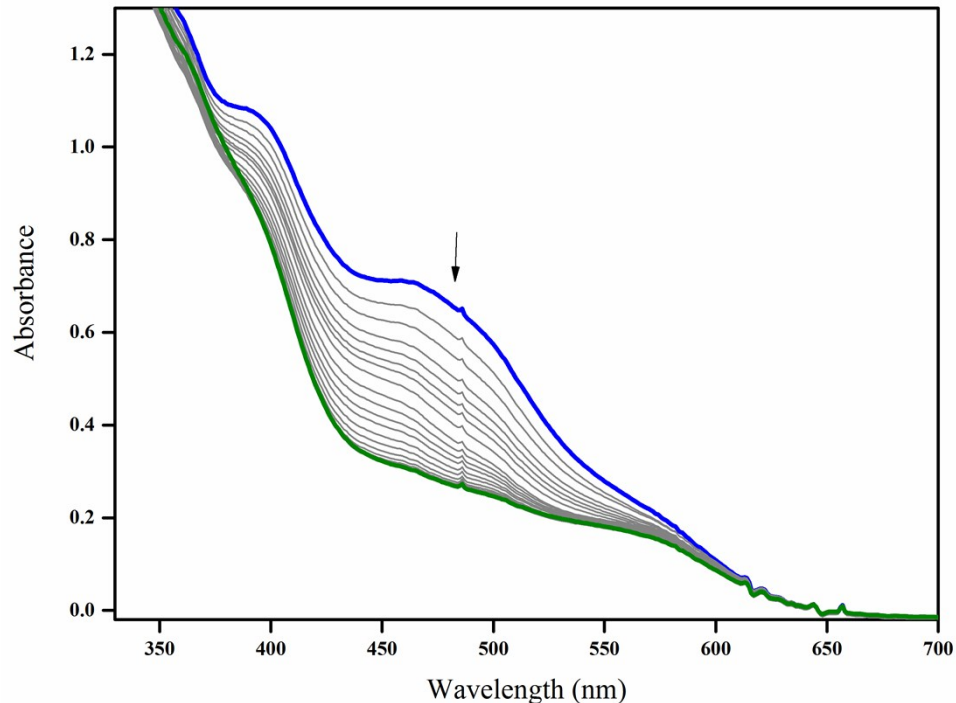


Figure S54. UV-Visible spectral changes for the reaction of **3b** (6×10^{-4} M) with ten equivalents of *tert*-butyl hydroperoxide and 0.5 equivalents of acetic acid at 25°C in acetonitrile\acetate buffer. The monitored disappearance of Fe(II) to acac MLCT band at 485 nm with 30 seconds time interval.

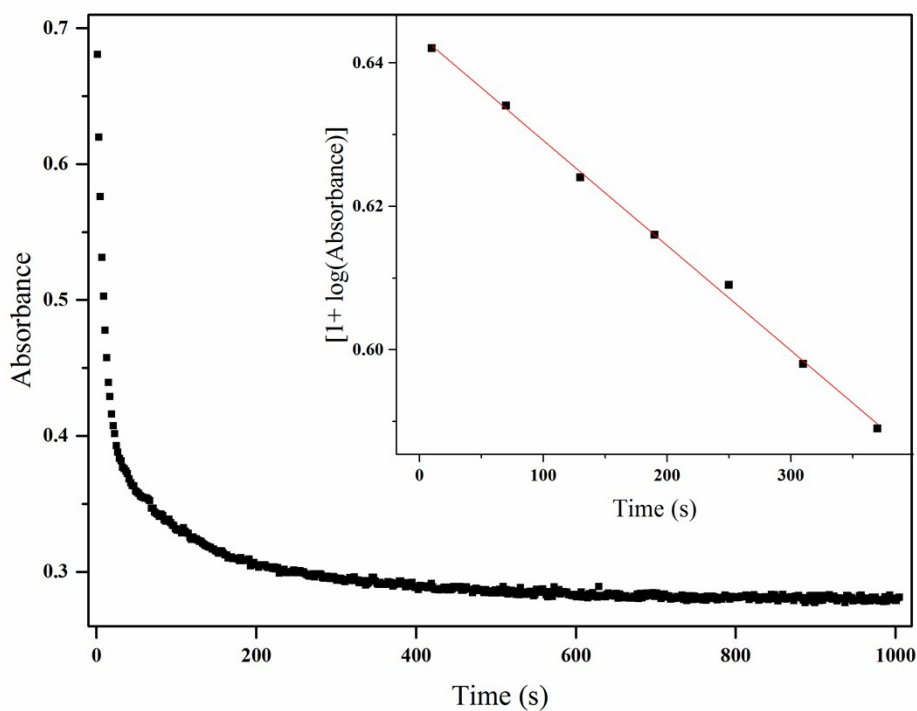


Figure S55. Plot of absorbance (485 nm) vs time for the reaction of **3b** (6×10^{-4} M) with ten equivalents of *tert*-butyl hydroperoxide and 0.5 equivalents of acetic acid in acetonitrile at 25°C. Inset: Plot of $[1 + \log(\text{Absorbance})]$ vs time.

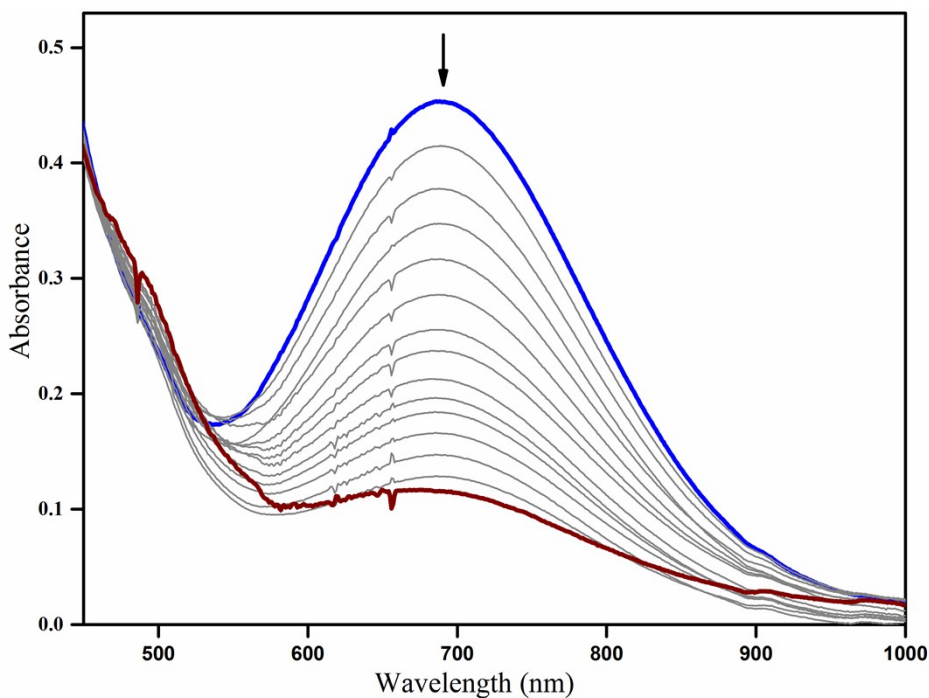


Figure S56. The UV-Visible spectral changes for the reaction of **2** (6×10^{-4} M) with ten equivalents of *tert*-butyl hydroperoxide in acetonitrile at 25°C. The monitored disappearance of Fe^{3+} -alkyl-peroxido species with a $t\text{-BuOO}^- \rightarrow \text{Fe}^{3+}$ LMCT band around 687 nm.

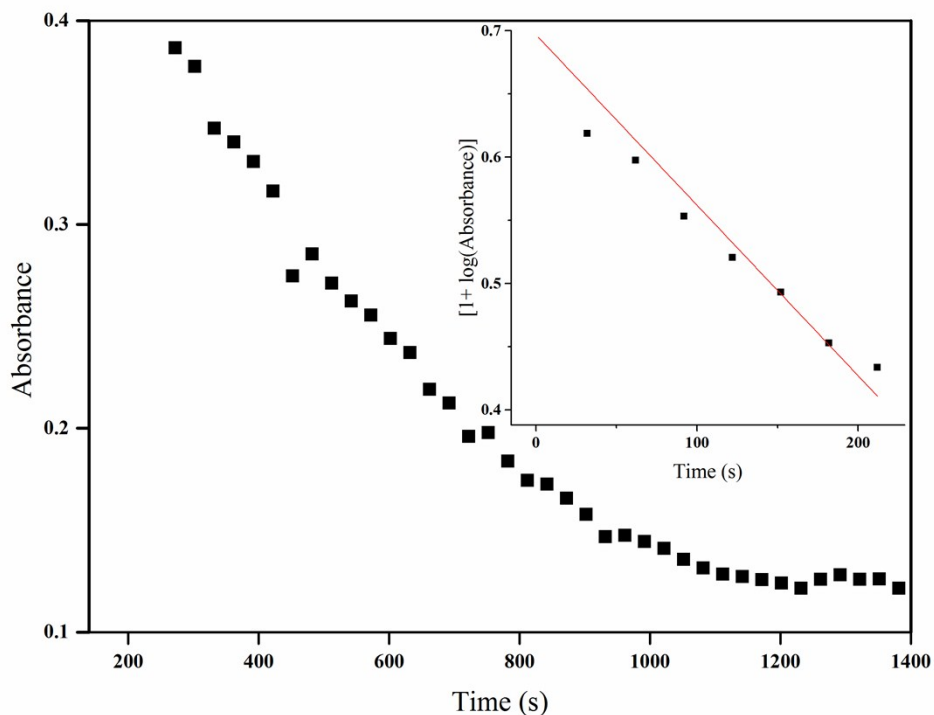


Figure S57. Plot of absorbance (687 nm) vs time for the reaction of $[\text{Fe}(\text{L}2)(\text{SO}_3\text{CF}_3)]\text{SO}_3\text{CF}_3$, **2** (6×10^{-4} M) with ten equivalents of *tert*-butyl hydroperoxide in acetonitrile at 25°C. Inset: Plot of $[1 + \log(\text{Absorbance})]$ vs time.

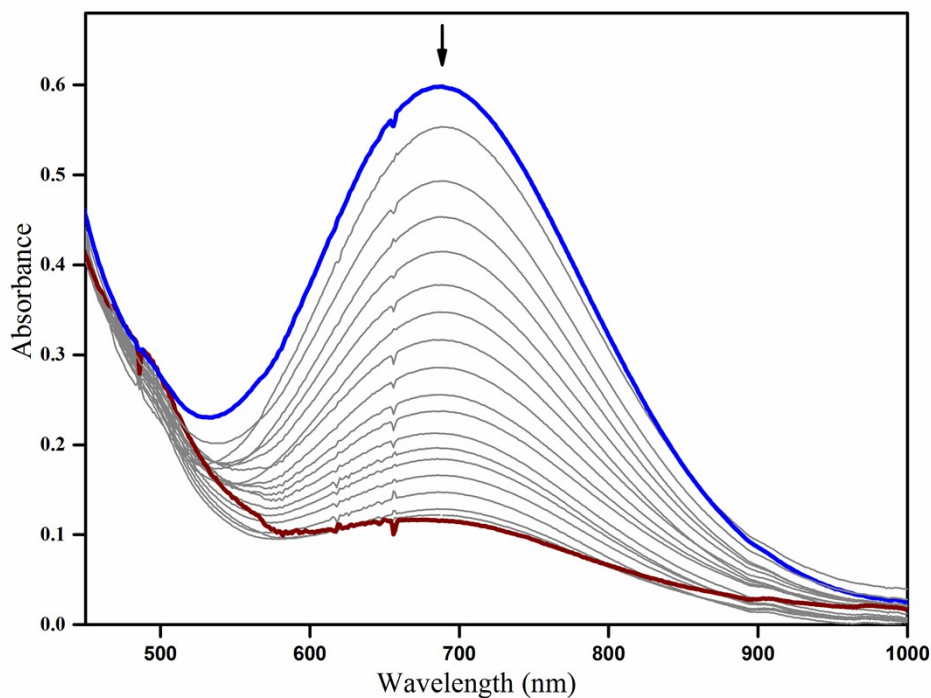


Figure S58. The UV-Visible spectral changes for the reaction of **3** (6×10^{-4} M) with ten equivalents of *tert*-butyl hydroperoxide in acetonitrile at 25°C. The monitored disappearance of Fe^{3+} -alkyl-peroxido species with a *t*-BuOO $^-$ \rightarrow Fe^{3+} LMCT band around 690 nm.

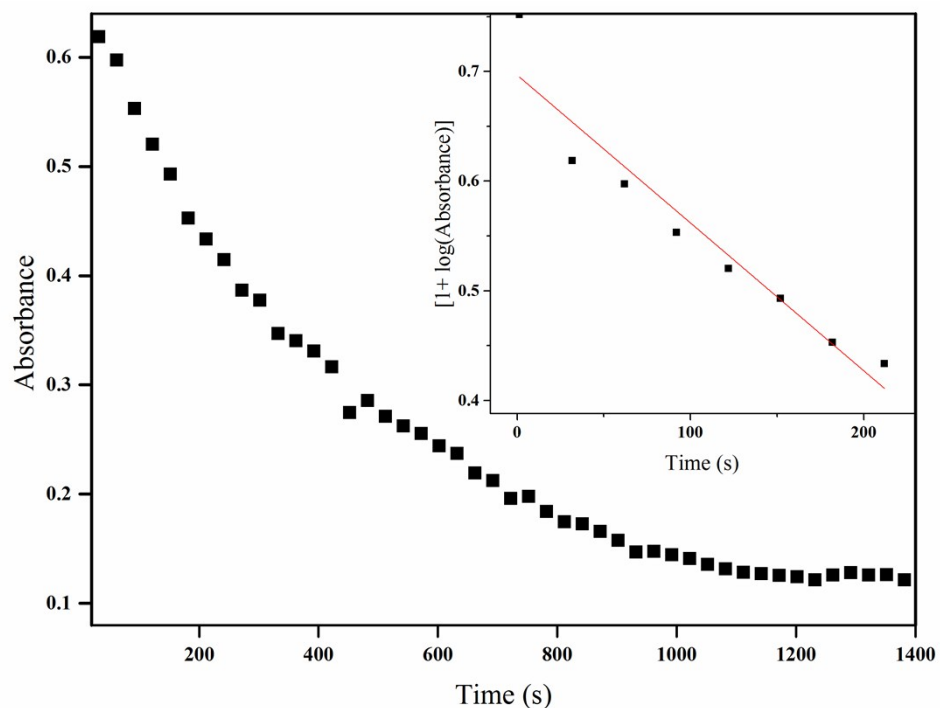


Figure S59. Plot of absorbance (690 nm) vs time for the reaction of **3** (6×10^{-4} M) with ten equivalents of *tert*-butyl hydroperoxide in acetonitrile at 25°C. Inset: Plot of $[1 + \log(\text{Absorbance})]$ vs time.

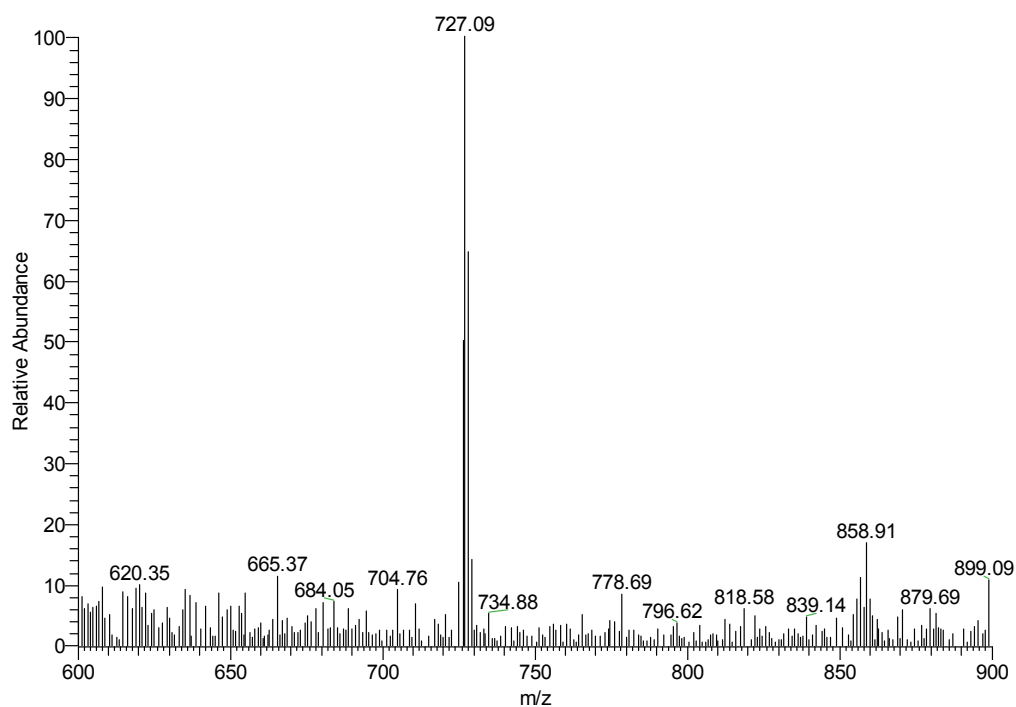


Figure S60. The ESI-MS spectra of $[\text{Fe}(\text{L}2)(\text{SO}_3\text{CF}_3)]\text{SO}_3\text{CF}_3$, **2** with *t*-BuOOH in acetonitrile.

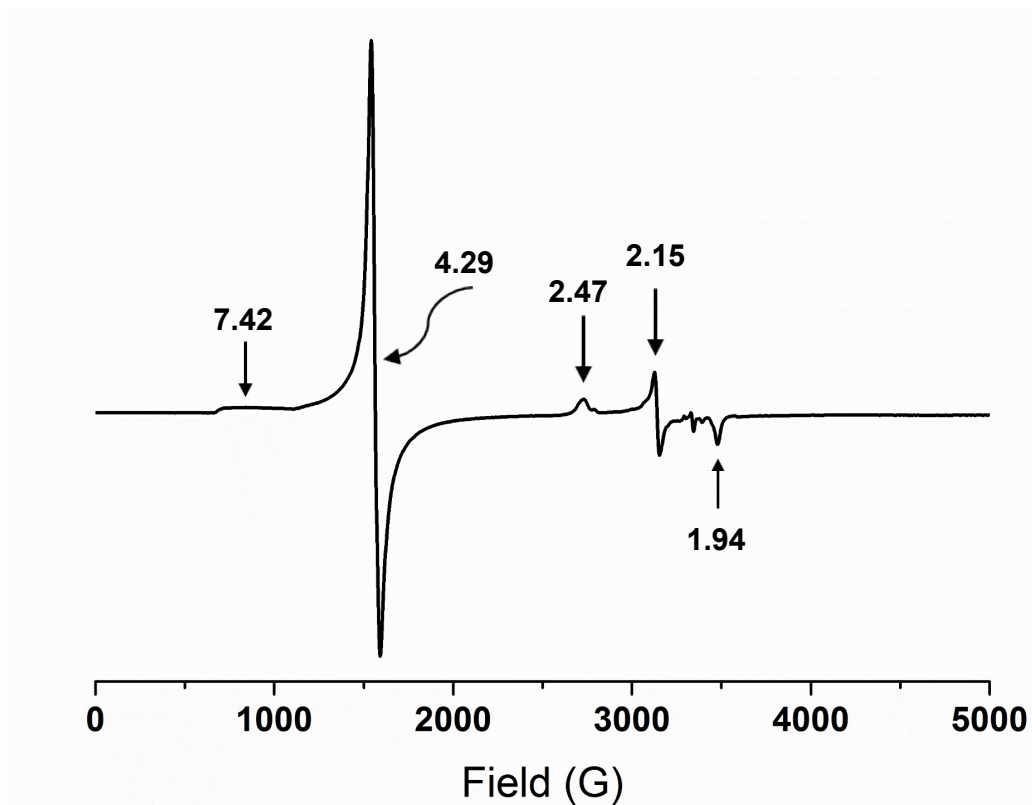


Figure S61. X-band EPR spectrum of **3** on treating with *t*-BuOOH. EPR Parameters: frequency for A, 9.3959; B, 9.3979; C, 9.3966; D, 9.3878 GHz; power = 0.63 mW; modulation amplitude=10 G; modulation frequency = 100 kHz; T = 10 K.

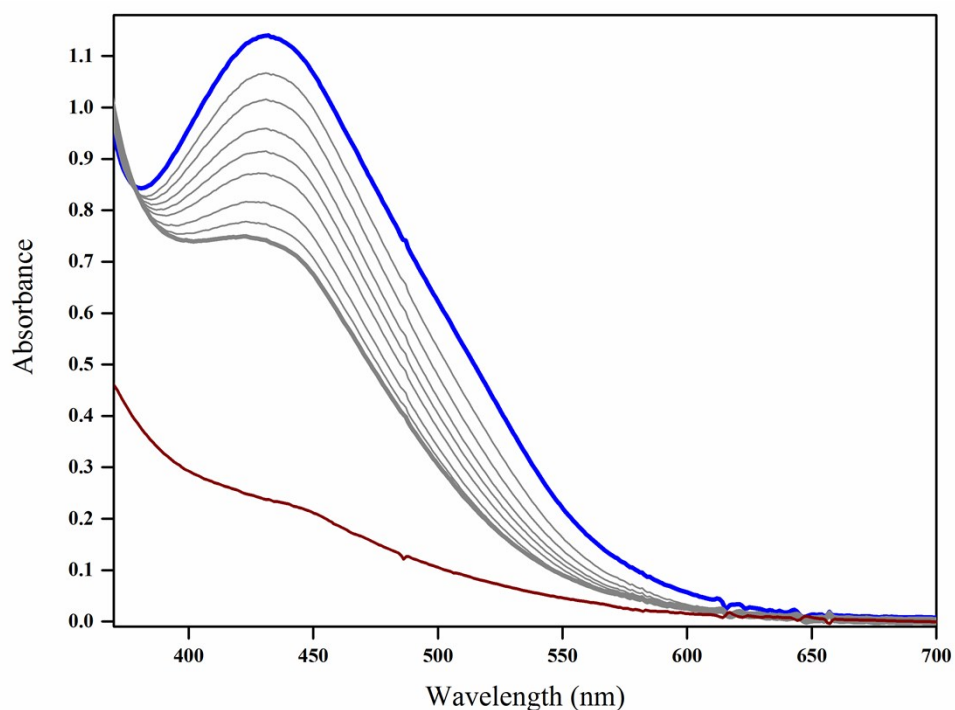


Figure S62. Progress of the reaction of **1a** (6×10^{-4} M) with 2 equivalents of $\text{PhI}(\text{OAc})_2$ and 0.5 equivalents of acetic acid at 25°C in acetonitrile/acetate buffer. The monitored disappearance of Fe(II) to acac MLCT band at 430 nm with 15 seconds time interval.

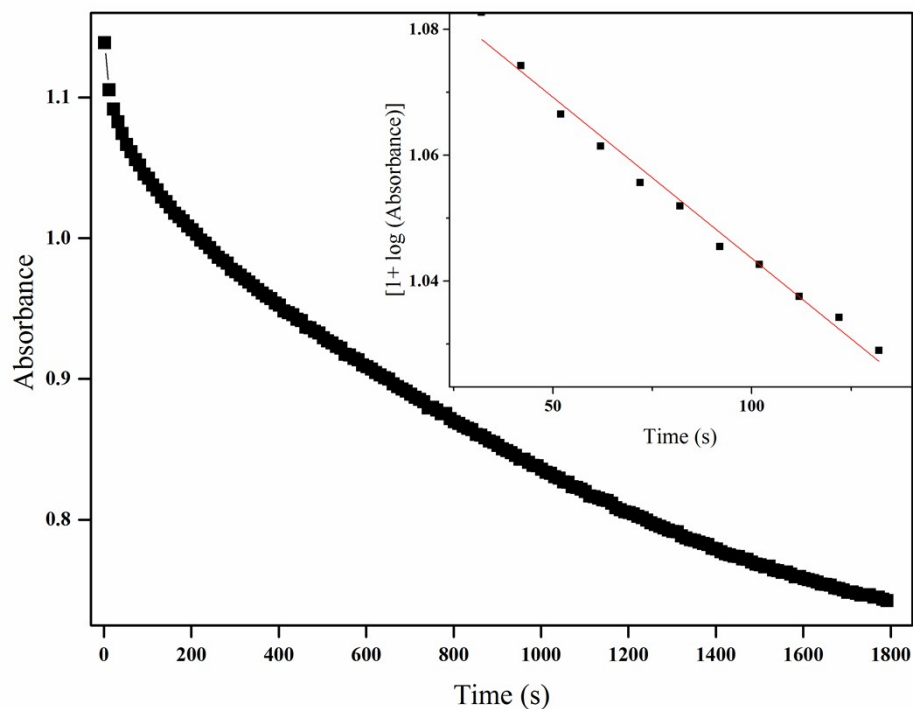


Figure S63. Plot of absorbance (430 nm) vs time the reaction of **1a** (6×10^{-4} M) with 2 equivalents of $\text{PhI}(\text{OAc})_2$ and 0.5 equivalents of acetic acid at 25°C . Inset: Plot of $[1 + \log(\text{Absorbance})]$ vs time.

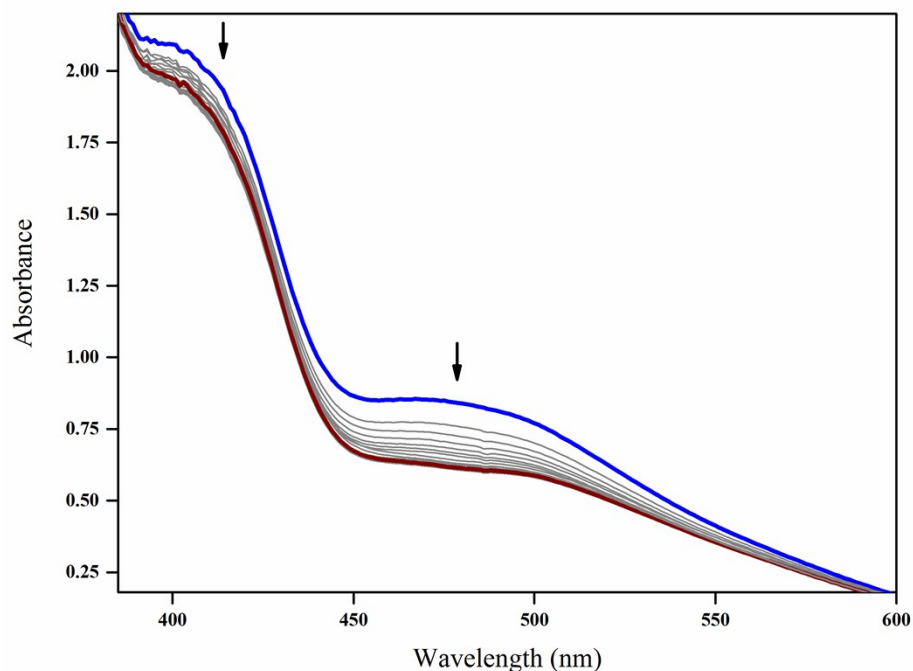


Figure S64. Progress of the reaction of **1b** (6×10^{-4} M) with 2 equivalents of $\text{PhI}(\text{OAc})_2$ and 0.5 equivalents of acetic acid at 25°C in acetonitrile/acetate buffer. The monitored disappearance of $\text{Fe}(\text{II})$ to acac MLCT band at 490 nm with 10 seconds time interval.

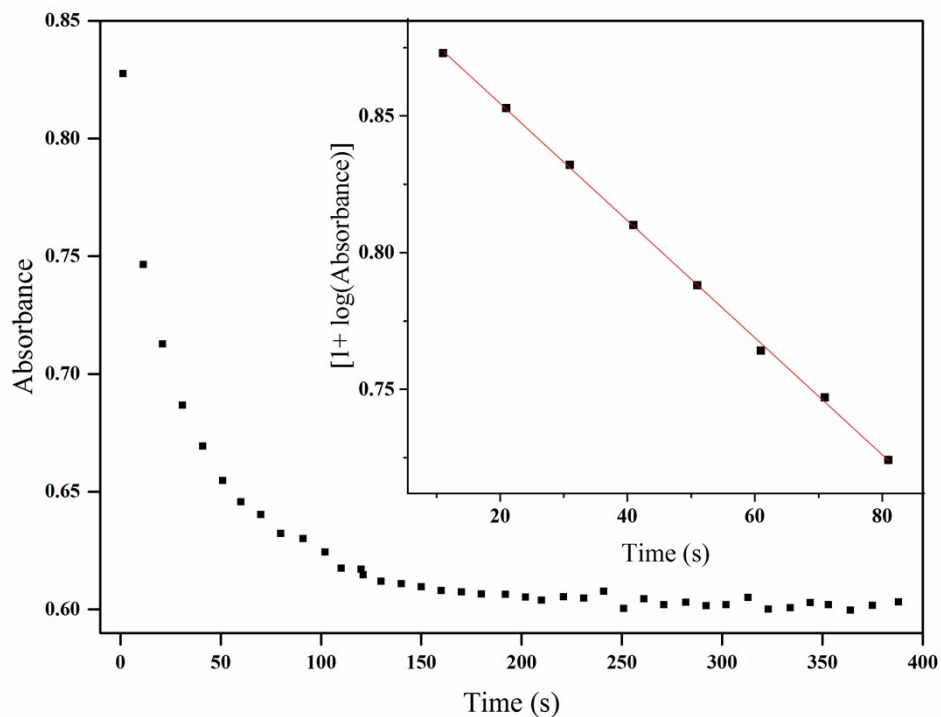


Figure S65. Plot of absorbance (490 nm) vs time the reaction of **1b** (6×10^{-4} M) with 2 equivalents of $\text{PhI}(\text{OAc})_2$ and 0.5 equivalents of acetic acid at 25°C . Inset: Plot of $[1 + \log(\text{Absorbance})]$ vs time.

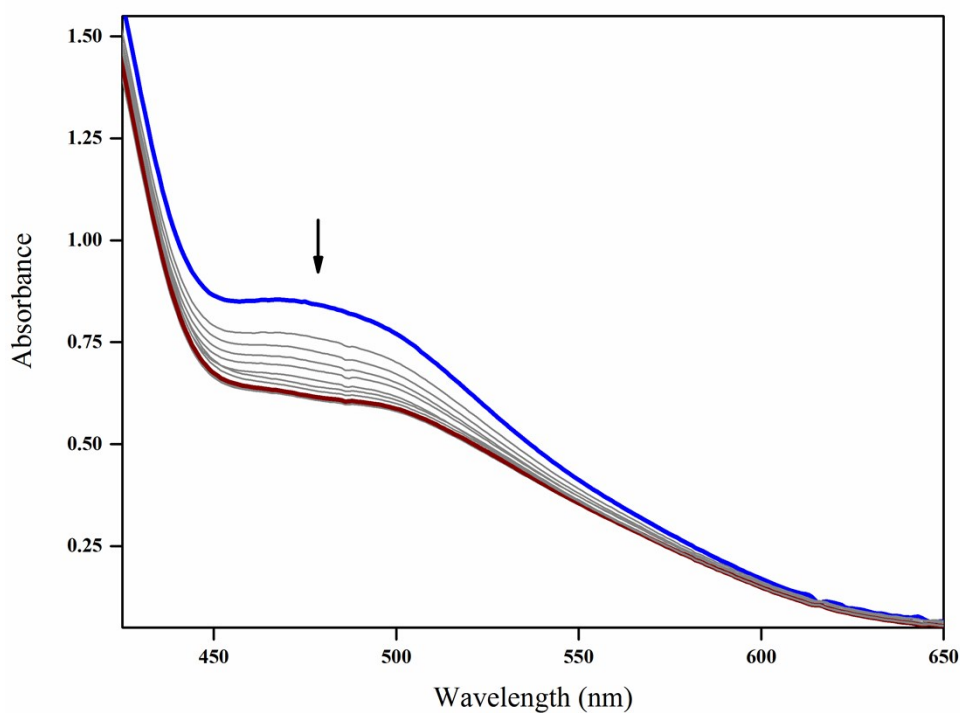


Figure S66. Progress of the reaction of **2b** (6×10^{-4} M) with 2 equivalents of $\text{PhI}(\text{OAc})_2$ and 0.5 equivalents of acetic acid at 25°C in acetonitrile/acetate buffer. The monitored disappearance of Fe(II) to acac MLCT band at 480 nm with 15 seconds time interval.

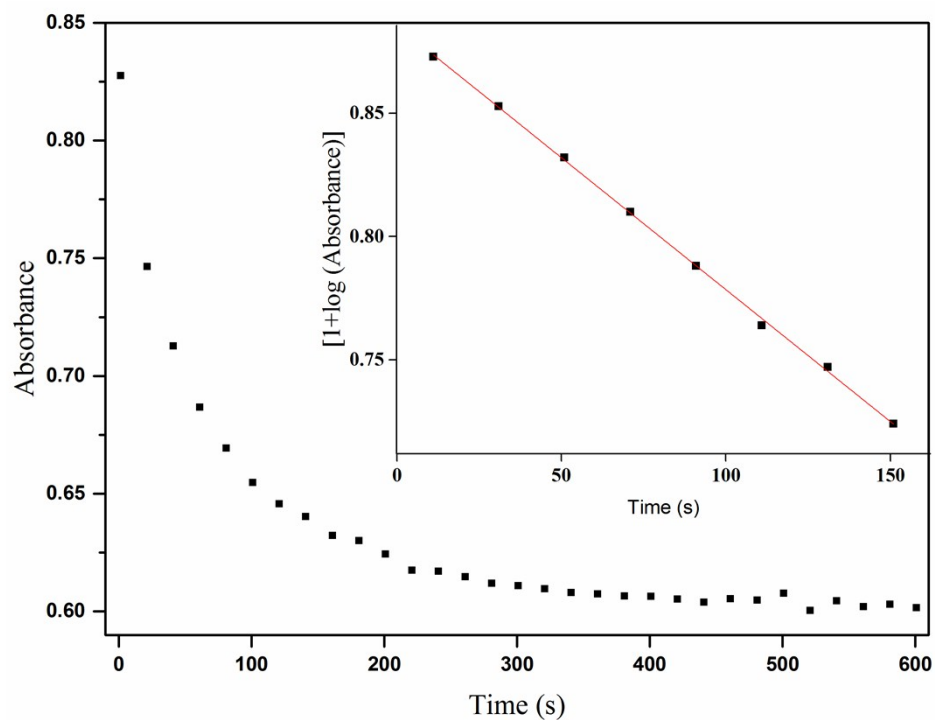


Figure S67. Plot of absorbance (480 nm) vs time the reaction of **2b** (6×10^{-4} M) with 2 equivalents of $\text{PhI}(\text{OAc})_2$ and 0.5 equivalents of acetic acid at 25°C . Inset: Plot of $[1 + \log(\text{Absorbance})]$ vs time.

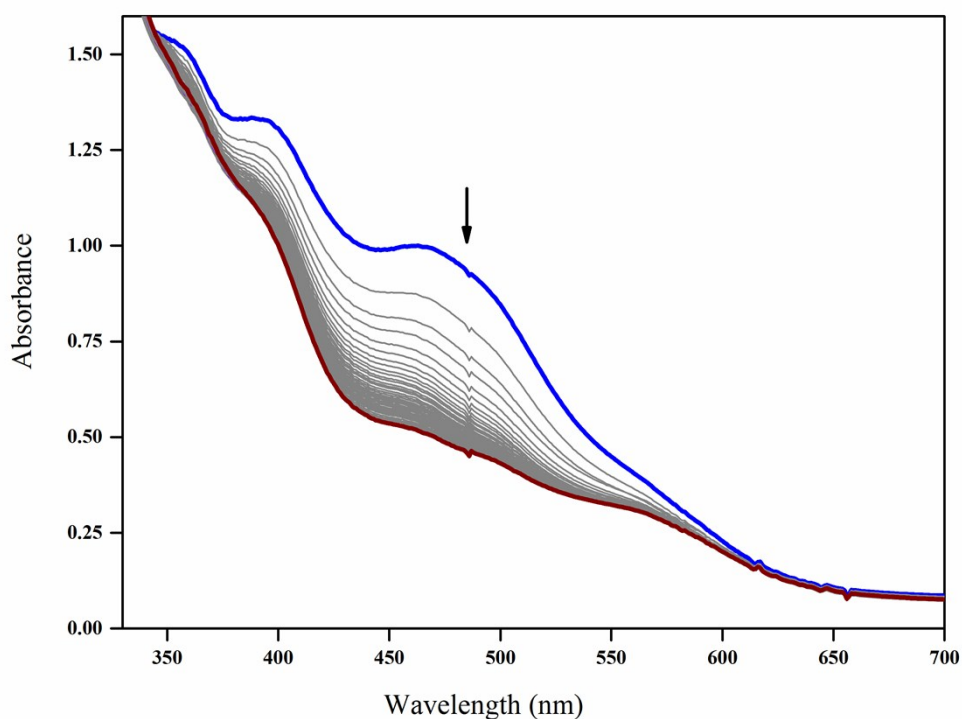


Figure S68. Progress of the reaction of **3b** (6×10^{-4} M) with 2 equivalents of $\text{PhI}(\text{OAc})_2$ and 0.5 equivalents of acetic acid at 25°C in acetonitrile/acetate buffer. The monitored disappearance of Fe(II) to acac MLCT band at 485 nm with 25 seconds time interval.

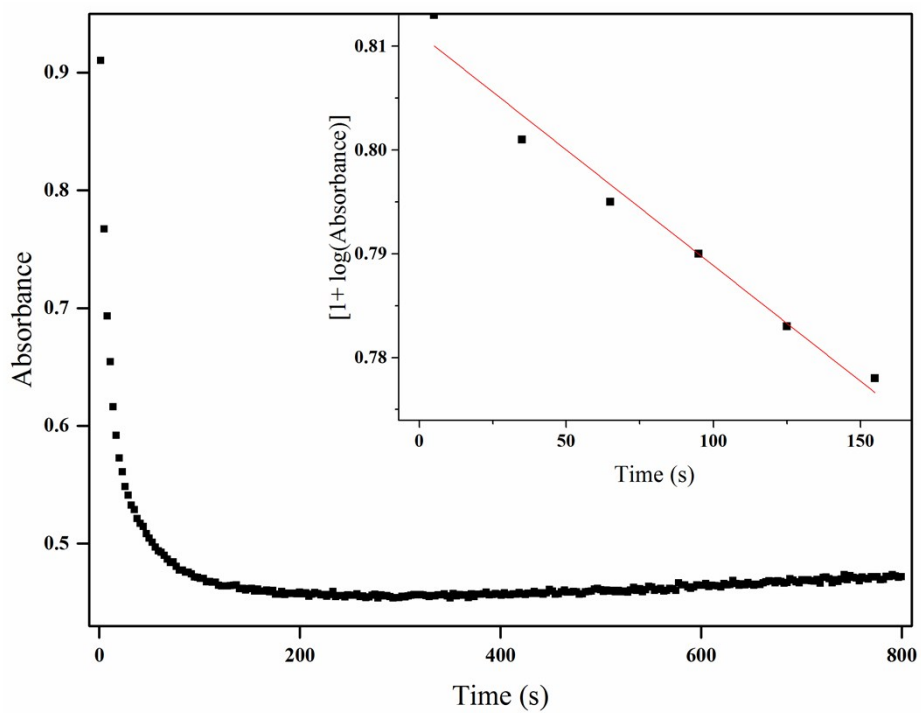


Figure S69. Plot of absorbance vs time the reaction of **3b** (6×10^{-4} M) with 2 equivalents of $\text{PhI}(\text{OAc})_2$ and 0.5 equivalents of acetic acid at 25°C . Inset: Plot of $[1 + \log(\text{Absorbance})]$ vs time.

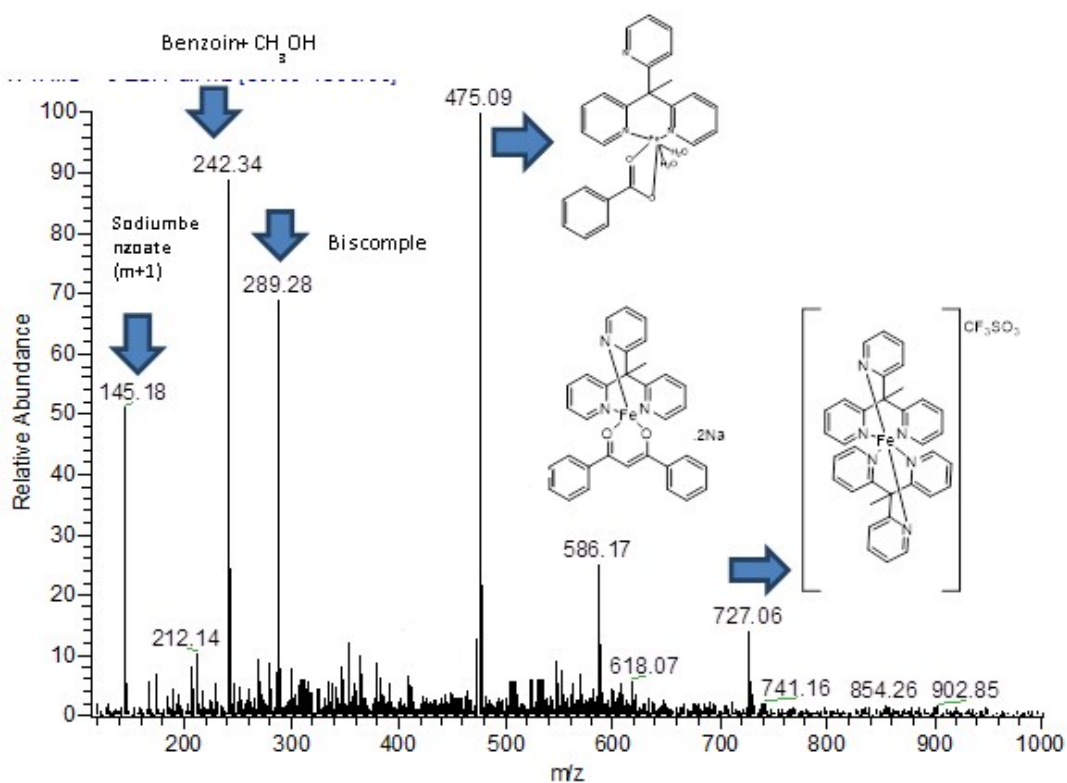
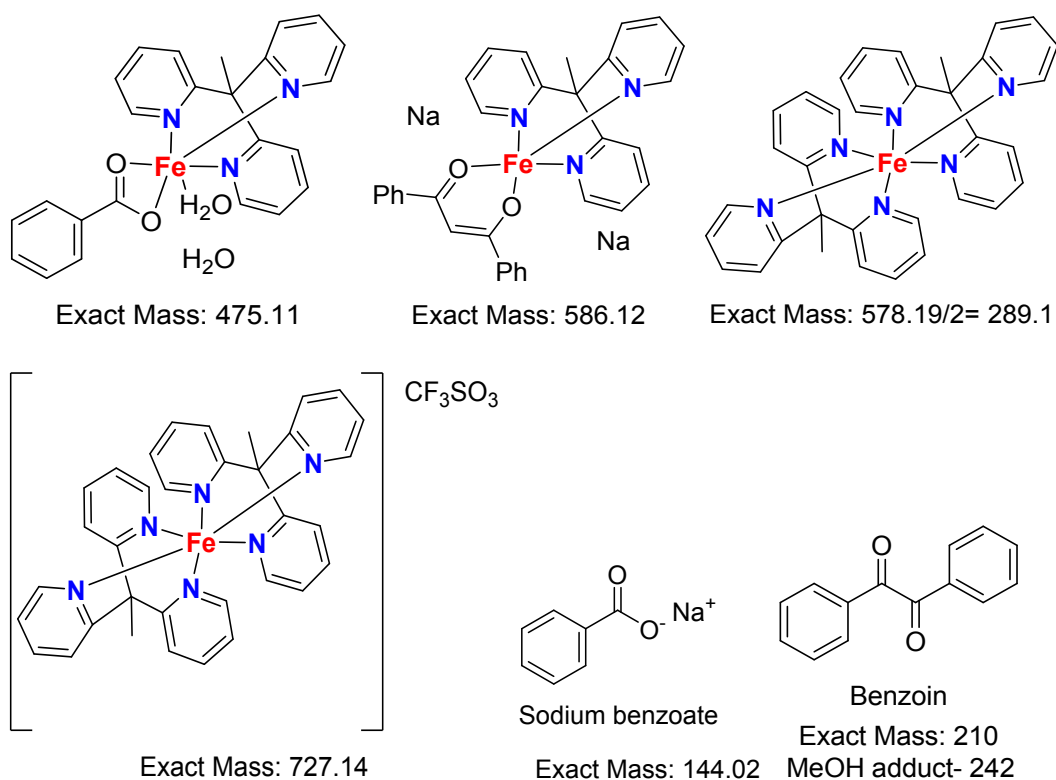


Figure S70. ESI- MS spectra in methanol for deoxygenation reaction mixture of **1b**.



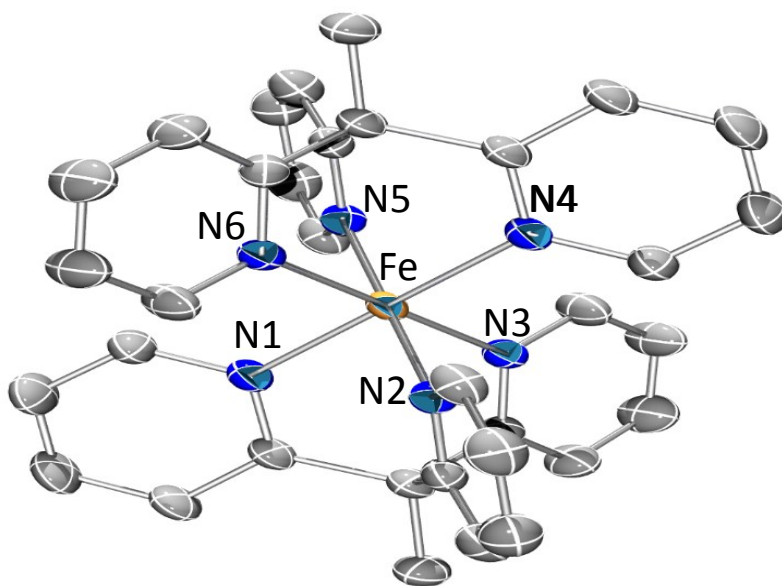


Figure S71. The molecular structure of $[\text{Fe}(\text{L1})_2](\text{CF}_3\text{SO}_3)_2$, H atoms and SO_3CF_3^- ions are omitted for clarity.

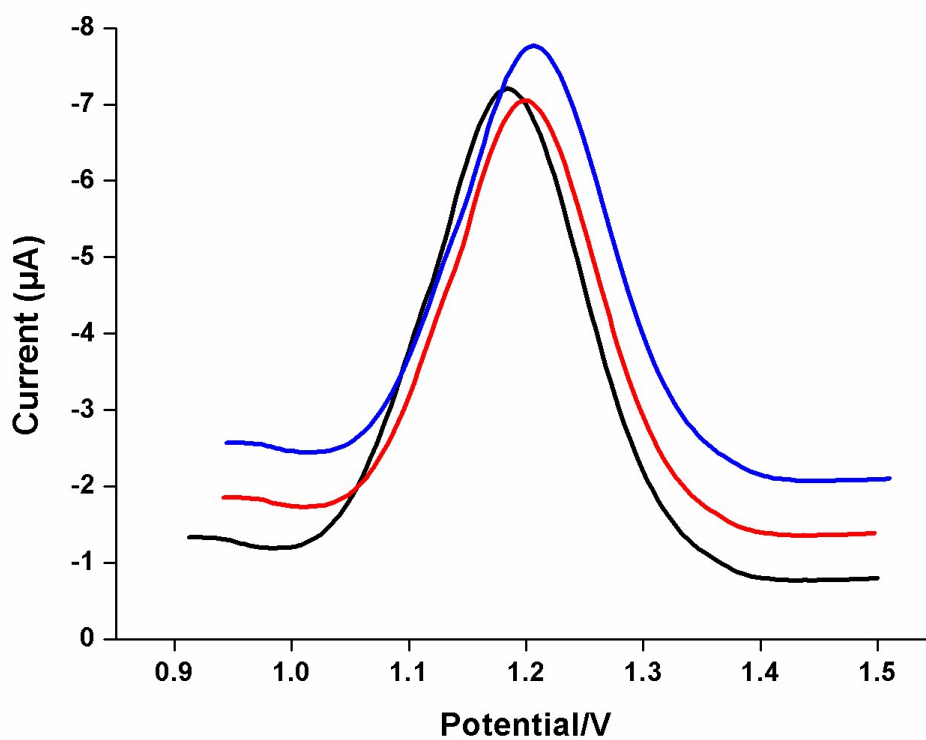


Figure S72. Time-dependent Differential pulse voltammetry (1×10^{-3} M) of **3a** with O_2 .

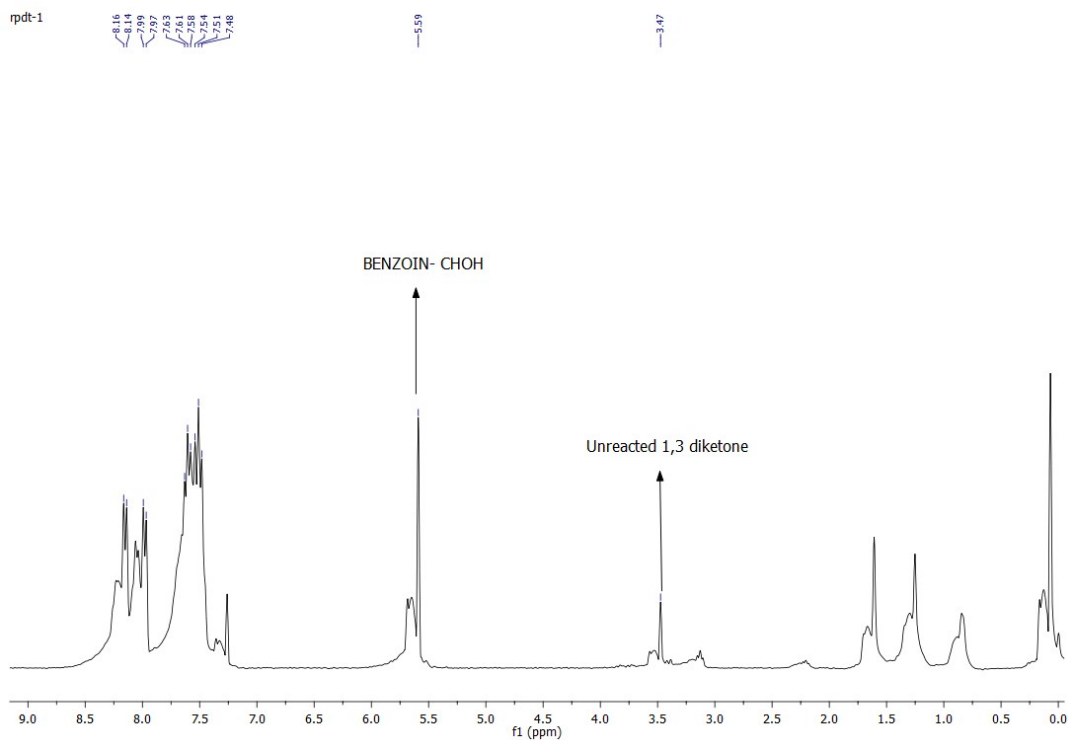


Figure S73. The ^1H -NMR spectra in CDCl_3 for the reaction mixture of **1b** with O_2 in presence of 0.5 equivalents acetic acid.

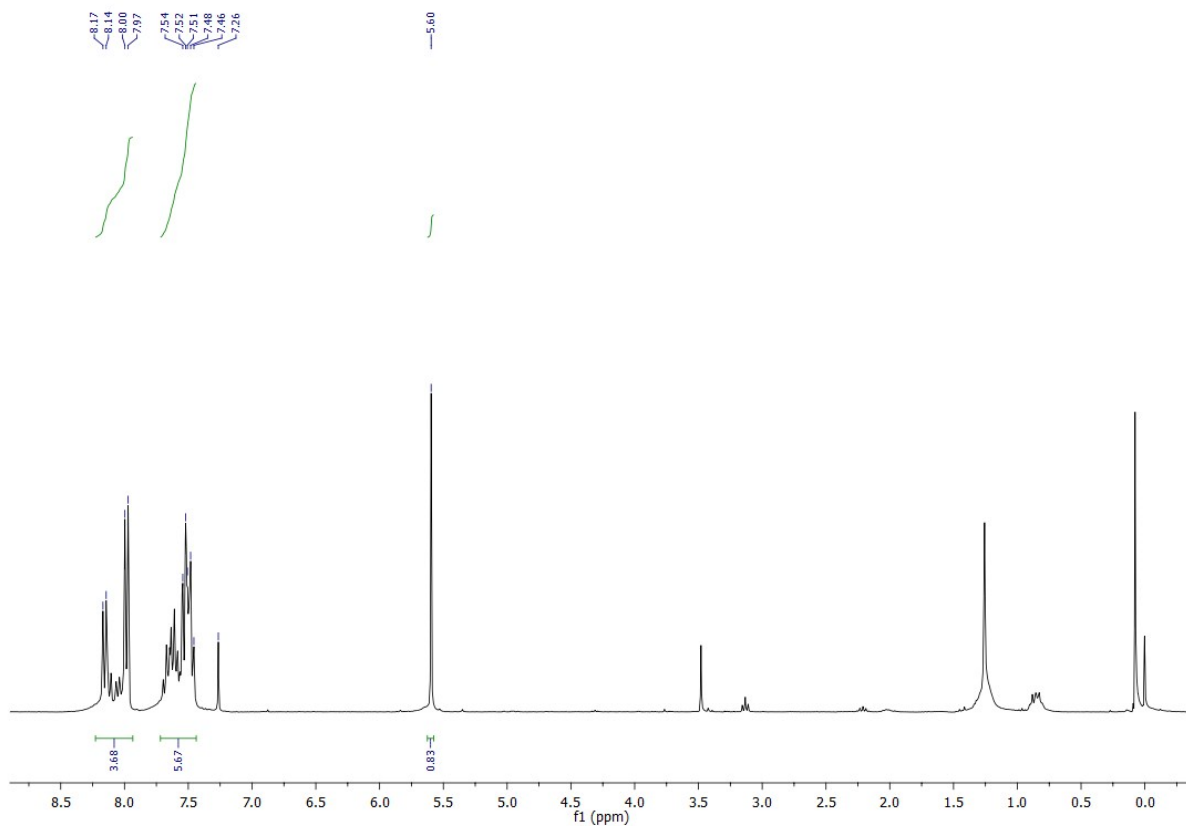


Figure S74. The ^1H -NMR spectra in CDCl_3 for one of the oxidative cleavage products benzoin from the reaction of **1b** with O_2 in presence of 0.5 equivalents acetic acid.

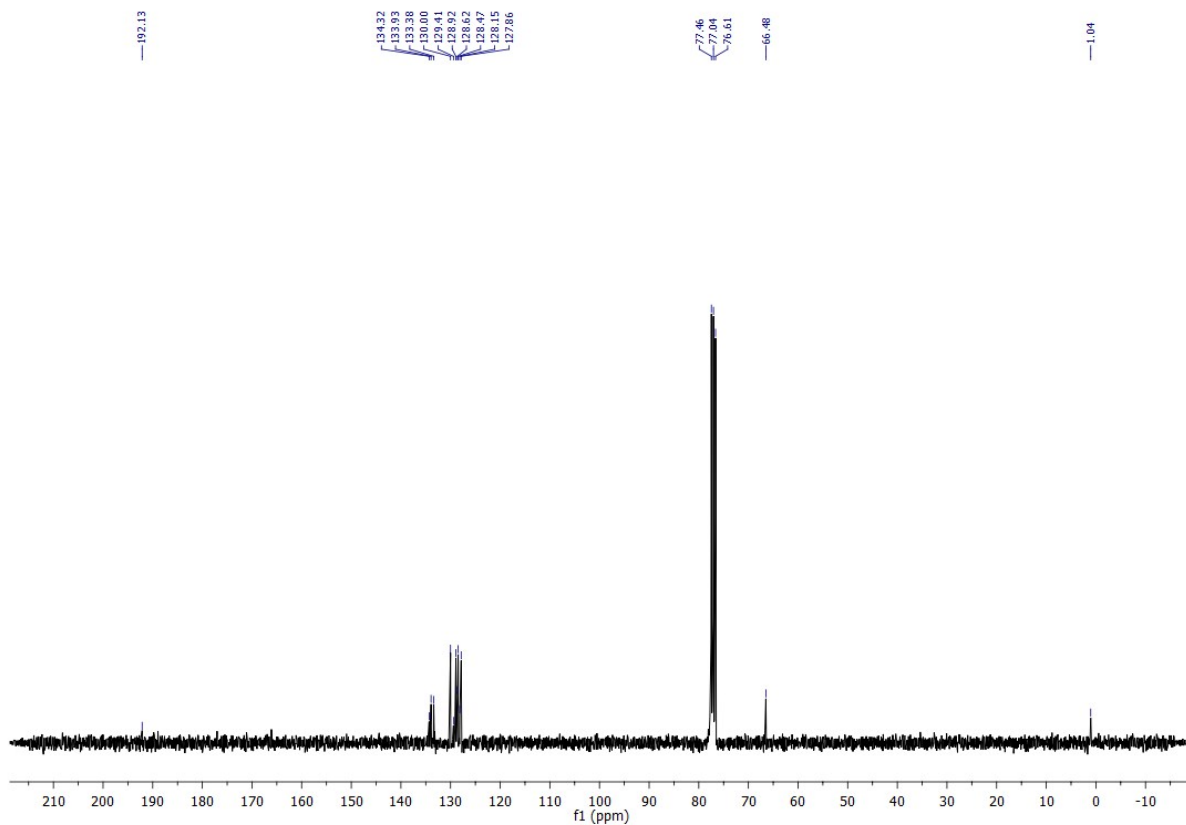


Figure S75. The ¹³C-NMR spectra (CDCl₃) for one of the oxidative cleavage products benzoin obtained from **1b**.

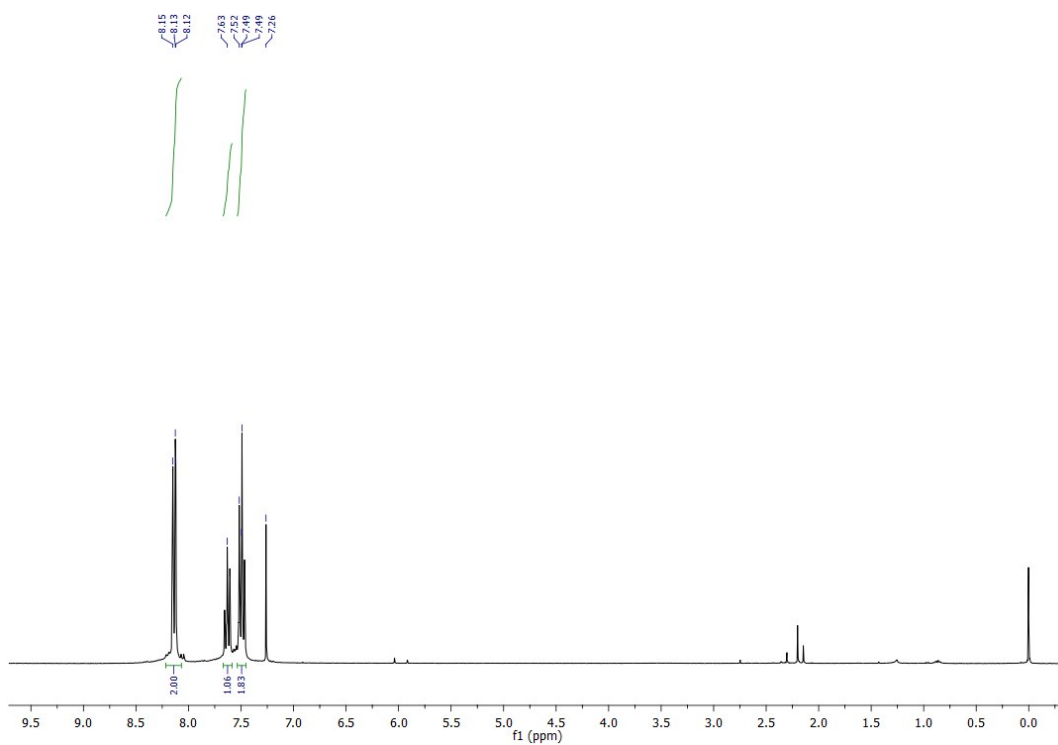


Figure S76. The ¹H-NMR spectra (CDCl₃) for one of the oxidative cleavage products benzoic acid obtained from **1b**.

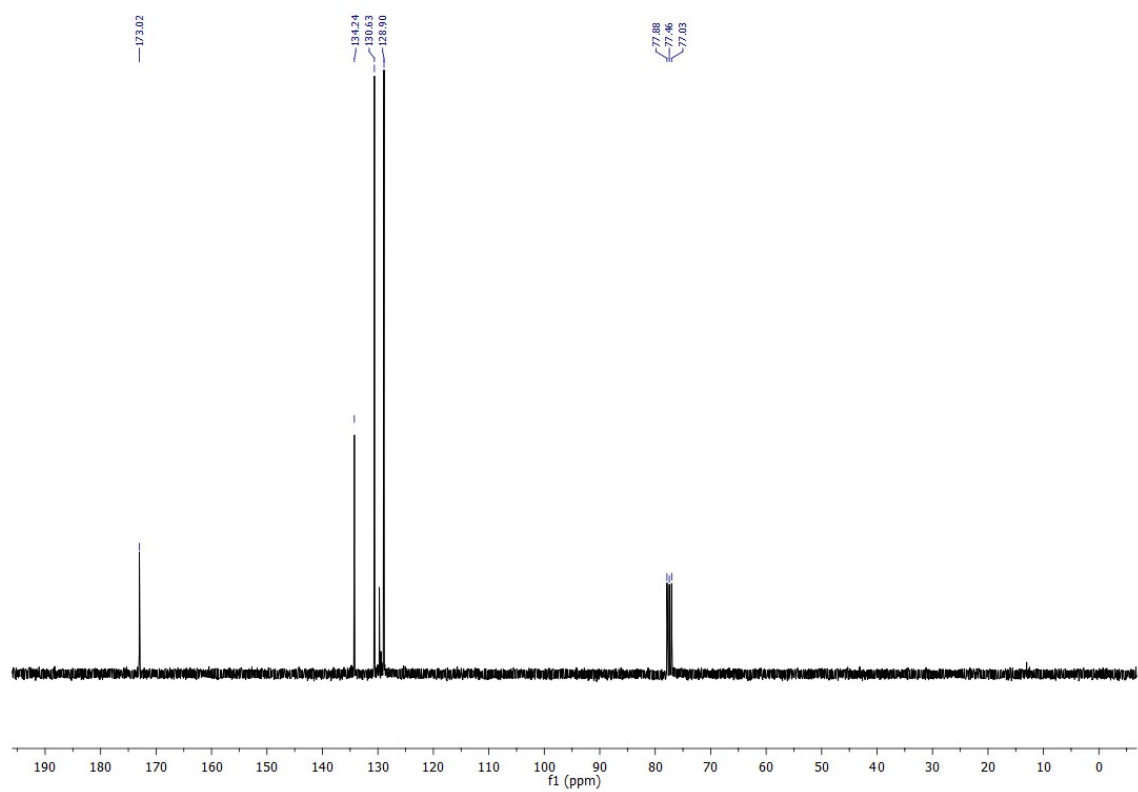


Figure S77. The ¹³C- NMR spectra (CDCl₃) for one of the oxidative cleavage products benzoic acid obtained from **1b**.

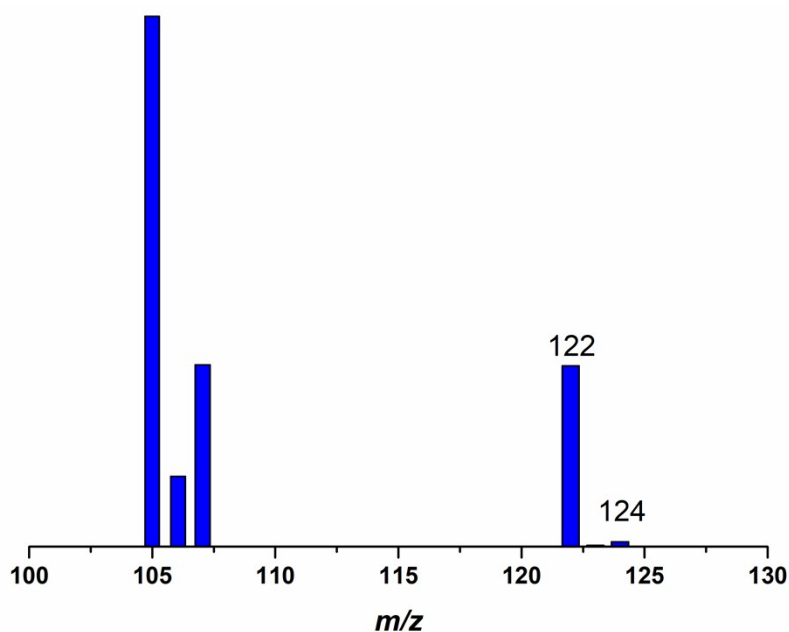


Figure S78: The dioxygen reaction for the reaction of Na(acac^{Ph}) with **1** using $^{16}\text{O}_2$ in H_2^{18}O .

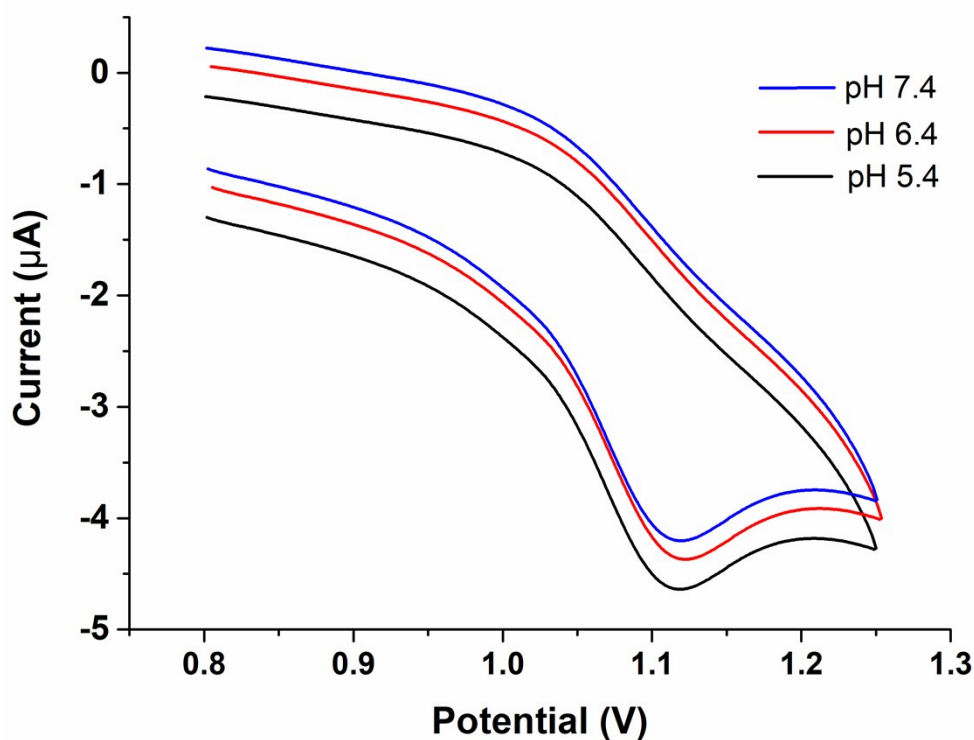


Figure S79: pH dependent cyclic voltammetry (CV) for $[\text{Fe}(\text{L}1)(\text{acac}^{\text{Me}})]\text{SO}_3\text{CF}_3$, **1a** (1×10^{-3} M) using TBAP (0.1 M) as supporting electrolyte in acetonitrile. Ag(s)/Ag⁺ (0.01 M, 0.10 M TBAP) as reference electrode. Platinum disc and platinum wire were used as working and counter electrodes respectively. Scan rate: 100 mVs^{-1} .

Table S1. Crystal data and structure refinement for [Fe(L1)(CH₃CN)₃](SO₃CF₃)₂ **1**

Empirical formula	(C ₂₃ H ₂₄ FeN ₆ ⁺²) ₂ (CF ₃ O ₃ S ⁻) ₄ · C ₂ H ₃ N
Formula weight	1517.99
Temperature	100K
Radiation and wavelength	MoK _α , 0.71073 Å
Crystal system	Triclinic
Space group	P 1
Unit cell dimensions:	a= 11.8586(6) Å α= 60.817(2)° b= 12.4140(6) Å β= 83.284(2)° c= 12.6961(6) Å γ= 73.222(2)°
Volume	1561.69(14) Å ³
Z	1
Density (calculated)	1.614 Mg/m ³
Absorption coefficient μ	0.704 mm ⁻¹
F ₀₀₀	774
Crystal size	0.31 x 0.26 x 0.13 mm
θ range for data collection	2.53 to 28.00°
Reflections collected / unique	13837 / 10107
R(int), R(sigma)	0.0227, 0.0407
Observed reflections [I > 2σ (I)]	9675
Index ranges ^s h, k, l	-15 ... 15, -15 ... 16, -16 ... 16
Completeness to θ = 28.0°	98.5%
Absorption correction	semi-empirical from equivalents
Max. and min. transmission	0.7457 and 0.5999
Structure Solution Program	SHELXS-97 (Sheldrick, 2008)
Structure Refinement Program	SHELXL-97 (Sheldrick, 2008)
Unit cell determination	2.61° < Θ < 28.58°
Data / restraints / parameters	10107 / 19 / 870
Goodness-of-fit on F ²	1.045
Final R indices [I > 2σ (I)], R(F), wR(F ²)	R1 ^a = 0.0400, wR2 ^b = 0.1117
Final R indices (all data) R(F), wR(F ²)	R1 ^a = 0.0417, wR2 ^b = 0.1129
Absolute structure parameter	0.30(2)
Difference density: rms, max, min	-0.507 e/Å ³ and 0.846
Diffractometer	Bruker APEX-II CCD, Dual, MoK _α
X-ray source	fine-focus sealed tube

$$^a R1 = \frac{\sum |F_o| - |F_c|}{\sum |F_o|}$$

$$^b R2 = \left\{ \frac{\sum w[(F_o^2 - F_c^2)]}{\sum w[(F_o^2)]} \right\}^{1/2}$$

Table S2. Kinetic data^a and product analysis^b for oxidative cleavage of **1- 3b** in CH₃CN

Complex	Oxygen source	$k_{\text{obs}} (\times 10^{-5} \text{ s}^{-1})$	$k_{\text{O}_2} (\times 10^{-3} \text{ M}^{-1} \text{ s}^{-1})$	$t_{1/2} (\text{h})^a$	Cleavage products (%) ^b
1a	O ₂	7.34 ± 0.02	9.41 ± 0.09	2.62	ND
1a	O ₂ /CH ₃ COOH	360.18 ± 0.47	460 ± 0.66	0.05	ND
2a	O ₂	3.83 ± 0.014	4.92 ± 0.07	5.02	ND
2a	O ₂ /CH ₃ COOH	133.33 ± 0.36	170.28 ± 0.50	0.14	ND
3a	O ₂	4.20 ± 0.01	5.37 ± 0.09	4.58	ND
3a	O ₂ /CH ₃ COOH	86.32 ± 0.29	110.24 ± 0.21	0.22	ND
1a	<i>t</i> -BuOOH ^c	159.25 ± 0.11	-	0.12	ND
1a	<i>t</i> -BuOOH ^c /CH ₃ COOH	412.3 ± 0.21	-	0.04	ND
2a	<i>t</i> -BuOOH ^c	63.25 ± 0.11	-	0.304	ND
2a	<i>t</i> -BuOOH ^c /CH ₃ COOH	212.5 ± 0.37	-	0.09	ND
3a	<i>t</i> -BuOOH ^c	72.25 ± 0.11	-	0.26	ND
3a	<i>t</i> -BuOOH ^c /CH ₃ COOH	156.6 ± 0.48	-	0.12	ND
1a	PhI(OAc) ₂ ^d /CH ₃ COOH	140.3 ± 0.28	-	0.13	ND
2a	PhI(OAc) ₂ ^d /CH ₃ COOH	78.27 ± 0.19	-	0.24	ND
3a	PhI(OAc) ₂ ^d /CH ₃ COOH	81.73 ± 0.15	-	0.23	ND
1b	O ₂ /CH ₃ COOH	0.26 ± 0.01	0.332 ± 0.08	74.03	A(42), B (29)
2b	O ₂ /CH ₃ COOH	0.062 ± 0.03	0.079 ± 0.23	310.4	A(26), B (24)
3b	O ₂ /CH ₃ COOH	0.057 ± 0.02	0.0772 ± 0.15	337.7	A(18), B (22)
1b	<i>t</i> -BuOOH ^c	13.3 ± 0.02	-	1.45	B(42), C (46)
2b	<i>t</i> -BuOOH ^c	10.7 ± 0.01	-	1.79	B(34), C (35)
3b	<i>t</i> -BuOOH ^c	8.7 ± 0.06	-	2.21	B(31), C (29)
3b	<i>t</i> -BuOOH ^c /CH ₃ COOH	1.48 ± 0.01	-	13.0	A(26), B (28)
1b	PhI(OAc) ₂ ^d /CH ₃ COOH	4.79 ± 0.02	-	4.01	A(48), B (43)
2b	PhI(OAc) ₂ ^d /CH ₃ COOH	1.57 ± 0.02	-	12.2	A(31), B (34)
3b	PhI(OAc) ₂ ^d /CH ₃ COOH	1.27 ± 0.01	-	15.1	A(27), B (29)
1	<i>t</i> -BuOOH ^c	66.66 ± 0.15	-	0.29	-
2	<i>t</i> -BuOOH ^c	53.72 ± 0.14	-	0.35	-
3	<i>t</i> -BuOOH ^c	58.17 ± 0.12	-	0.33	-

^a $k_{\text{O}_2} = k_{\text{obs}}/[\text{O}_2]$. [O₂] in CH₃CN, 8.1×10⁻³ M; $t_{1/2} = 0.693/k_{\text{obs}}$; ^bIsolated yields; ^cten equivalents; ^dtwo equivalents. ND – not detected.

Table S3. pH dependent data for the reaction of $[\text{Fe}(\text{L}1)(\text{acac}^{\text{Me}})]^+$ for **1a**, (6×10^{-4} M) with saturated O_2 in aqueous acetonitrile (10% H_2O) in various pH (7- 5.1) at 25°C .

pH	$k_{\text{obs}} (\times 10^{-5} \text{ s}^{-1})$	$k_{\text{O}_2} (\times 10^{-3} \text{ M}^{-1} \text{ s}^{-1})$	$t_{1/2}$ (h)
7.4	7.34 ± 0.017	9.41 ± 0.085	2.62
7.0	9.83 ± 0.027	12.55 ± 0.102	1.958
6.7	43.78 ± 0.076	55.91 ± 0.102	0.439
6.3	136.4 ± 0.102	174.2 ± 0.117	0.141
5.7	251.2 ± 0.102	320.81 ± 0.21	0.0766
5.4	360.18 ± 0.47	460 ± 0.66	0.05
5.2	364.78 ± 0.32	465.8 ± 0.2	0.051
5.1	364.87 ± 0.12	465.8 ± 0.32	0.051

Table S4. The isolated yield of oxidative cleavage of catalysed by **1b**.

Substrate Equiv.	Oxygen Source	Time (h)	Isolated Yield (%)	
			With H^+	Without H^+
1	O_2	12	A(42), B (29)	-
1	<i>t</i> -BuOOH	3	A(47), B (41)	B (42), C (46)
2	<i>t</i> -BuOOH	6	A (38), B (46)	B (39), C (47)
1	$\text{PhI}(\text{OAc})_2$	3	A (48), B (43)	B (46), C (49)
2	$\text{PhI}(\text{OAc})_2$	6	A (32), B (44)	B (29), C (45)

Table S5. Time-dependent oxidative cleavage product analysis of **1b** with O_2 in CH_3CN .

S. No	Time (h)	Isolated Yield (%)
1	3	A(17), B (11)
2	6	A(29), B (19)
3	9	A (36), B (25)
4	12	A(42), B (29)